FINAL REPORT

FFG Projektnummer	878151	**FörderungsnehmerIn**	ÖBV
Bericht Nr.	1	**Berichtszeitraum**	01.01.2019 – 30.09.2020
Bericht erstellt von	Pauser, Robisson		

Richtwert für den Umfang: 10-20 Seiten

1. Ziele und Ergebnisse

- Wurden die dem Förderungsvertrag zugrunde liegenden Ziele erreicht?
  Sind diese Ziele noch aktuell bzw. realistisch?
  Achtung: Änderungen von Zielen erfordern eine Genehmigung durch die FFG.
- Vergleichen Sie die Ziele mit den erreichten Ergebnissen.
- Beschreiben Sie „Highlights“ und aufgetretene Probleme bei der Zielerreichung.

This second year’s achievements include:

- Setting up of rheology protocols to measure structuration of cement with time.
- Evaluation of elastic and loss moduli evolution with time on several binders (Portland cement, alkali-activated material, calcite). Highlight of the challenges to obtain reproducible and reliable data.
- Qualitative confirmation that rheology can be used to asses attractive forces between cement particles / early hydrates (C-S-H).
- Identification of an optimized pre-dry-mixing sequence for the production of UHPC using conventional mixers based on rheological and mechanical testing campaign. Deagglomeration of silica fumes (a nano-filler) was identified as the limiting step.
- Test campaign including shear strength, fracture energy and tensile strength measurements to characterize interfaces between old and new concrete using epoxy as a bonding agent. Results consistently show a decrease of strength and fracture energy with increasing temperature during the application of epoxy and the early curing of concrete.
- Year 2 detailed report sent to all partners.

A new PhD student, Subhransu Dhar, joined the group. Experimental results were obtained despite our lab move from Blamauergasse to Arsenal and the measures linked to COVID-19.

Team (co-authors of reports) is now composed of Dana Daneshvar, Karl Deix, Subhransu Dhar, Johannes Kirnbauer, Teresa Liberto, Agathe Robisson.

2. Arbeitspakete und Meilensteine

2.1 Übersichtstabellen

Erläuterung:
Die Tabellen sind analog zum Förderungsansuchen aufgebaut.

Basistermin: Termin laut Förderungsansuchen bzw. laut Vertrag gültigem Projektplan
Aktuelle Planung: Termin laut zum Zeitpunkt der Berichtslegung gültiger Planung

Tabelle 1: Arbeitspakete

AP No.	work package designation	Degree of completion	base date		Current		Achieved results / deviations
			start	end	start	end	
1	Project management	40%	10.18	09.23	10.18	09.23	Mid-year 2 meeting cancelled due to COVID-19. Set of slides with comments sent instead. End of year 2 meeting happened on-line.
2	State of the art	70%	10.18	09.19	10.18	09.23	Examination of EU legislation for recyclability in construction, foam cement, durability of recycled aggregate concrete continues with each step of the research projects.
3	Development of rheological tests and procedures	60%	10.18	09.21	10.18	09.23	Rheology protocols were investigated and demonstrate the importance of the sample preparation and the pre-shear step. We measured de-structuration of cement suspensions (shear stress during application of shear strain) and restructuration (elastic modulus during small strain oscillations). Results show that rheological measurements give quantitative reliable information about cement structuration at very early stage.
4	Investigation of the influence of the mixing process	80%	10.18	09.21	10.18	09.21	Focus on dry premixes for UHPC. UHPC pre-dry-mixed with intensive mixer and wet-mixed with conventional mixer show very good rheological and mechanical properties. Deagglomeration of silica fumes was identified as the limiting step in the process.
5	Influence of cement grain size distribution on concrete rheology foamability and setting properties	40%	10.18	09.20	10.18	09.20	Oscillatory rheology and fractal models of particle cohesiveness were used to compare an ordinary Portland cement -OPC-, an alkali-activated material -AAM- and a nano-calcite suspension. Rheology could qualitatively confirm that calcite suspension behavior is governed by weak long-

							range attractive forces (electrostatic) while OPC and AAM are governed by short range strong attractions.
6	Interfaces between old material and new concrete	40%	10.18	09.23	10.18	09.23	Influence of shrinkage on top cover was theoretically (analytically) assessed. Test campaign with old/new concrete with epoxy as bonding agent was run. The influence of temperature (from 5 to 55 °C) during the bonding and early curing was investigated. Shear strength, fracture energy and tensile strength were measured. Results are consistent, showing a decrease of strength and fracture energy with increasing temperature during the application of epoxy.
7	Device for measuring infiltration	10%	10.19	10.22	07.20	10.22	Project start was delayed due to COVID-19 (lab closed to all students and staff). Exploratory setup built with 2 size LECA beads and a low yield stress slurry. The slurry could infiltrate the pack of large (8-16 mm) but not infiltrate the same pack of the small (4-8mm) LECA beads. Concept of flow-controlled infiltration setup (from bottom) ready.
8	Equipment for the production of cement foams	100% / stopped	10.19	10.20	10.19	10.20	C-S-H was identified as a potential stabilizing foam agent. Preliminary tests were performed on a C-S-H paste. Capacities were partially relocated to AP 5 and AP 7.
9	Device for characterizing volume changes or limiting pressure of RA concretes	20%	10.19	10.23	10.19	10.23	Experiments are running. Tests are described in this report.
10	High thermal insulation in a double walled tower	0%	10.22	10.23	10.22	10.23	This work package starts in the last year of research

2.2 Description of the work carried out during the reporting period

- Describe the work carried out in the reporting period, structured according to the work packages.
- Were the work steps and packages developed according to plan?
  Were there any significant deviations?
- The description shall also include any change in the methodology used.
  Caution: Changes in methodology and significant changes in the work plan require approval by the FFG.

WORK PACKAGE 1
Project management

The control of the project execution was carried out.

Web-Meetings was organized with all those involved in the project and the interim results discussed.

WORK PACKAGE 2
State of the art

Examination of EU legislation for recyclability in construction, foam cement, durability of recycled aggregate concrete continues with each step of the research projects.

WORK PACKAGE 3
Development of rheological tests and procedures

Motivation

This project aims at assessing oscillatory rheology as a tool to study the chemico-physical bonding mechanisms responsible for the development of cementitious material's early strength. The focus of the current study is to perform oscillatory rheological measurements on cement pastes without the addition of any superplasticizer or other additives. This choice was made in order to investigate the properties of the cement itself and more precisely of the network that forms due the attractive forces between particles in the early hydration (i.e. a few minutes after the initial mixing). As shown by previous studies [1-3], macroscopic elastic properties are related to the microscopic structure. In the case of cement, in the first minutes after mixing, a series of complex chemical reaction takes place [4]. The mechanism of these dissolution-precipitation reactions are still under debate. With this study, we aim at contributing to this discussion from a new perspective: oscillatory rheology.

In this report, we present both the study of a reliable testing protocol and the early results. Cement pastes with two different w/c ratio are characterized and tested fresh and after 20 minutes. A cement powder without C_3A (tricalcium aluminate) was chosen. This choice was made to focus on the effect of calcium silicate hydrate (C-S-H) formed upon the hydration of the silicate phases (C_3S and C_2S) and investigate the cement cohesion due to the net attraction between C-S-H surfaces (i.e. ionic and electrostatic forces) [4-6].

Materials and methods

Cement suspensions were prepared by dispersing Portland cement CEM I (Contragress cement powder 42.5 R-SR 0 WT 27 C_3A-free, Lafarge-Holcim) in distilled water with w/c ratio of 0.35 and 0.40. A vortex stirrer (Ultra Turrax Tube Drive P control Workstation, IKA) is used to prepare 10 ml of homogeneous cement paste. During mixing, cement powder is slowly added to distilled water and a spatula is used to scrape the cement at the wall tube. Then a continuous mixing step of 3 minutes at 3000 rpm is applied.

Two different cement slurries are tested: *fresh* and *after 20 minutes*. The *fresh* sample is immediately loaded on the rheometer after the mixing step . The *after 20 minutes* one is put to rest for 20 minutes and then mixed again for 3 minutes at 3000 rpm before loading.

We use an Anton Paar rheometer (MCR 302) with different geometries: serrated (PP25/P2) and sand-paper coated (P320, 46 μm) parallel plates both with a top diameter of 25 mm. The two geometries are chosen to prevent wall slip between the plates and the cement paste. The gap between the plates is 2 mm and a moisture chamber is used to prevent water evaporation during the experiment. A constant temperature of 20 °C is set. A schematic of the experimental setup is shown in Fig. 3.1 [7]. The data were analyzed and plotted using Matlab and Origin software's. The experimental protocol is fully detailed in the next section.

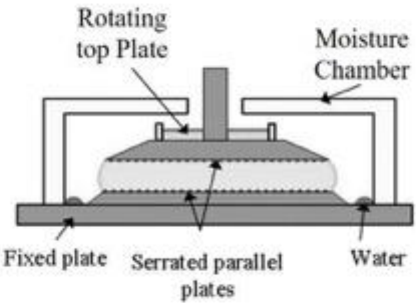

Fig. 3.1: Sketch of the experimental setup [7]: parallel plates profiled geometry with moisture chamber

Extensive protocol study

As per the literature, an intensive study on cement oscillatory rheology is yet to be done. Cement rheological properties depend on numerous parameters such as (a) physical factors such as w/c ratio, cement particle size; (b) chemical factors such as presence of aluminates (i.e. C_3A), minerals or second-raw constituents; (c) preparatory phase like mixer type, time and rate/energy of mixing.

In order to proceed with oscillatory rheology of cement pastes, going deeper into the understanding of our measurement protocol is necessary. The experimental protocol consists of three steps, namely conditioning, measurement and control. These steps are discussed in detail in the following sections.

Influence of pre-shear

The shear history on a cement suspension has a great impact on its rheological properties. Cement samples with different shear histories do not exhibit similar behavior during rheological measurements [8,9]. Hence, it is important to select an appropriate step to have reproducible measurements. We name this step the "conditioning step". The conditioning step consists of: pre-shear (PS) and time structuration (TS1) as sketched in Fig. 3.2.

Cement is largely made up of C_3S which reacts with water to form hydrates, mainly C-S-H. These C-S-H particles form bridge-like contact points between the cement particles. As more time is given to the cement to hydrate, more of these contact points are created which in-turn increases the strength and elastic modulus of the cement [5,6,10]. At early times, most of these C-S-H contacts can be broken down and reformed, giving cement its thixotropic behavior.

In this phase of the study, we want to analyze the effect of PS type (rotational, oscillatory) and duration. Consecutively, we study the regrowth of such structures during TS1, by measuring the growth of elastic modulus.

This study on pre-shear effect was performed on cement pastes at different ages (fresh, after 20 minutes) and w/c (0.40, 0.35). Each experiment is repeated in two independent campaigns (new mix).

The PS is used to ”reset” (break the structure) and homogenize the sample between the plates. This can be done either by imposing an oscillatory or a rotational shear. For oscillatory pre-shear (OPC), we apply two different strain amplitudes (γ = 10% & γ = 100%) for three different durations (0 s, 30 s and 300 s). For the amplitude γ = 100%, we have also measured the effect of 60 s of pre-shear.

For rotational pre-shear (RPC), two different shear rates are used: 1 s^{-1} and 10 s^{-1}, for three time durations (3, 30 and 300 s).

After both OPS and RPS, a time structuration step (TS1) is imposed on the sample by maintaining a low strain amplitude of 0.001% for 300 s (and also 30 s for OPS at γ = 100%). During this resting time, the material can restore the interparticle interactions that were destroyed during the pre-shear step, and thus recovers rigidity (elastic modulus increases).

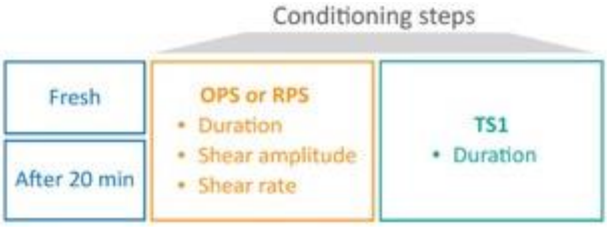

Fig. 3.2: Sketch showing the conditioning steps for both ”fresh” and ”after 20 minute” samples

Solid-like behavior of cement paste

Based on the results obtained, we found that the OPS of 100% gave a more reliable and reproducible data. Keeping OPS of 100% and TS1 of 300 s, we define the complete protocol to measure the rest or solid-like behavior of cement paste. The protocol consists of: conditioning steps (oscillatory pre-shear, OPS, time structuration, TS1), measuring step (amplitude sweep, AS), and a control step (time structuration, TS2). This protocol was applied to cement pastes at different ages (fresh, after 20 minutes) and w/c (0.40, 0.35), as shown in Fig. 3.3. Each experiment is repeated for two independent trials.

Strain amplitude sweep (AS) consists in subjecting the sample to increasing strain amplitude cycles. It characterizes the sample both in its solid state (“at rest”) at small strain amplitudes, and during its transition from a solid to a liquid-like behavior at higher strain amplitudes. In our AS, strain is gradually applied from extremely low amplitude 0.001% to as high as 100%, in a continuous ramp, logarithmic in time.

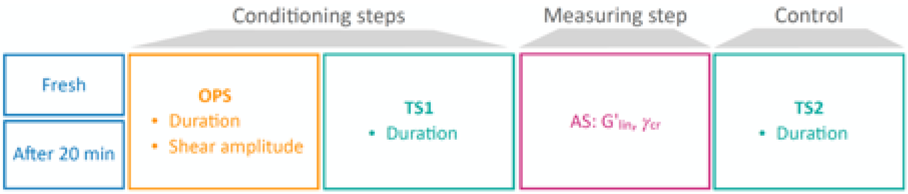

Fig. 3.3: Sketch showing the complete protocol on fresh and after 20 min samples. An oscillatory pre-shear (OPS) of γ = 100% is applied in the conditioning step of the measurements.

Fig. 3.4 shows a typical AS curve for cement paste. For low strain amplitude γ, both the elastic, G′ and viscous moduli, G″ remain nearly constant and G′ is higher than G″ which suggests a solid-like behavior. At the end of this plateau, as γ increases, both moduli drop and the cement paste enters in the liquid-like regime. In order to characterize the system at rest, we average, in the linear region, the largest G′ with its two nearest neighbors, defining it as G'_{lin}. The value of γ for which G′ drops (end of linearity) is defined as critical strain, γ_{cr}. We quantify γ_{cr} as the strain corresponding to 80% of G'_{lin}, as shown in Fig. 3.4.

The last step of this protocol is called "Control" and consists of a time structuration TS2 that follows the same protocol as TS1 with a fixed duration of 300 s. TS2 is made to keep track of the cement strength recovery after the amplitude sweep.

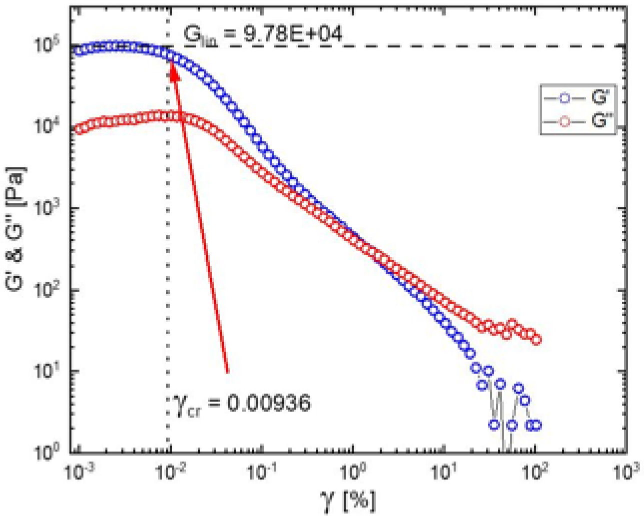

Fig. 3.4: Variation of elastic and viscous modulus, G' and G", by gradually increasing the strain amplitude from 0.001 % to 100%. Blue dots represents elastic modulus and red ones represents

viscous modulus. G'_{lin} represents the average value of G' in the initial plateau and γ_{cr} represents critical strain

Results

Influence of pre-shear

The stress evolution with time for both OPS and RPS is shown in Fig. 3.5. As expected, the shear stress of the system reduces with time (particle-particle contacts are broken down). Note that the data with OPS γ = 10% are made with parallel plates coated with sand paper (P320). The general trend in all the steps is maintained for both geometries.

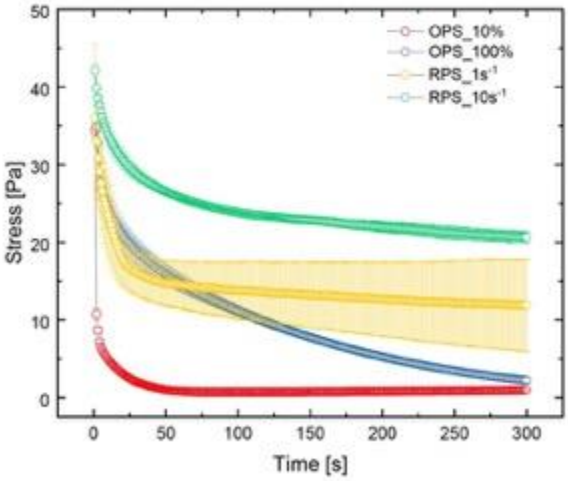

Fig. 3.5: Shear stress as a function of time for different pre-shear conditions (red : OPS - 10 %, blue : OPS - 100 %, yellow : RPS - $1s^{-1}$, green : RPS - $10s^{-1}$)

In Fig. 3.6, the time structuration steps TS1 after OPS for fresh and after 20 min cement (w/c = 0.4) are compared. We observe that the longer the duration of the pre-shear phase, the slower the structuration (increase of G′ modulus). Moreover, the G′ values of the cement after 20 min is generally lower for all PS values as compared to the fresh cement.

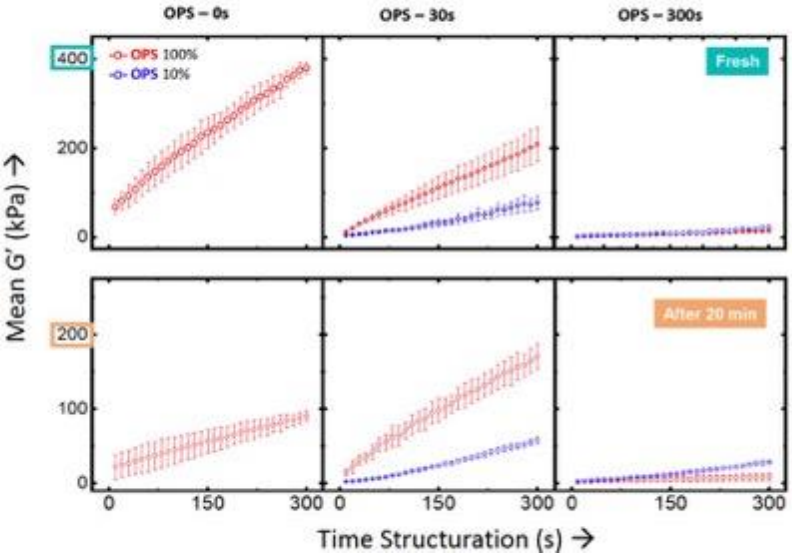

Fig. 3.6: Mean elastic modulus as a function of time structuration by varying the pre-shear duration. OPS: Red - 100 % and blue - 10 %. The top three graphs are for fresh samples and the bottom three for samples after 20 min.

Also, note that in Fig. 3.6, the red circles data were obtained with OPS of strain amplitude 100% (using serrated parallel plates) and the blue circles for strain amplitude 10% (using sand paper P320 coated parallel plates). This tends to show that sand paper may result on more slip than serrated plates.
Each data point is averaged over two independent tests. Similar trends are also observed for w/c = 0.35 (not shown in the report).

Fig. 3.7 shows the effect of rotation pre-shear (RPS) on time structuration TS1. Despite changing both intensity and duration of RPS, we could not observe a significant change in the TS1. In fact, the final value of G′ obtained after RPS of 1 s^{-1} (green data) for the three time durations is similar to the values for rotational PS of 10 s^{-1} (orange data). Similar considerations can be made for after 20 min samples, although there is an overall decrease of G′, as observed for OPS.

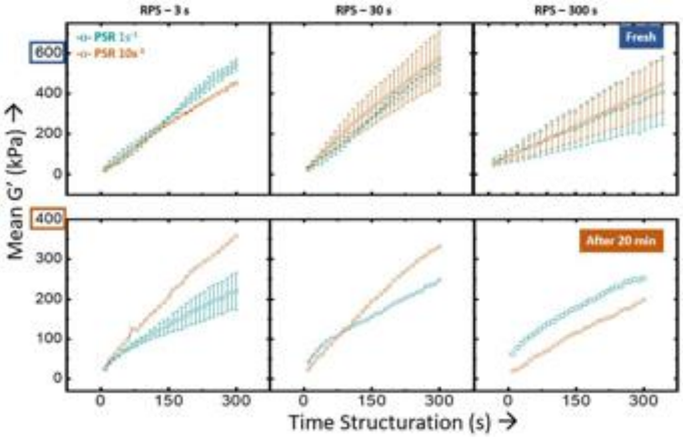

Fig. 3.7: Mean elastic modulus as a function of time structuration by varying the rotational pre-shear duration. Green: RPS = 1 s^{-1} and orange: RPS = 10 s^{-1}. The top three graphs are for fresh samples and the bottom three for samples after 20 min.

Measuring step

In Fig. 3.8 left, we show the evolution of G'_{lin} with PS duration for fresh cement and cement after 20 min, for two TS of 30 s and 300 s. The linear storage modulus G'_{lin} decreases with PS time and is always higher for fresh cement than cement after 20 min. Moreover, G′ for TS 300 s is always higher than TS 30 s (as expected). A similar trend is also observed for a w/c ratio of 0.35 (not shown in the report).
In Fig. 3.8 right, the dependence of γ_{cr} on OPS duration for two different sample ages and TS1 durations, is shown. The critical strain γ_{cr} remains almost constant for PS duration between 0 s and 60 s, whereas there is a slight increase for a PS of 300 s for

both fresh and after 20 min samples. A similar trend is also obtained for w/c ratio of 0.35 (not shown in the report).

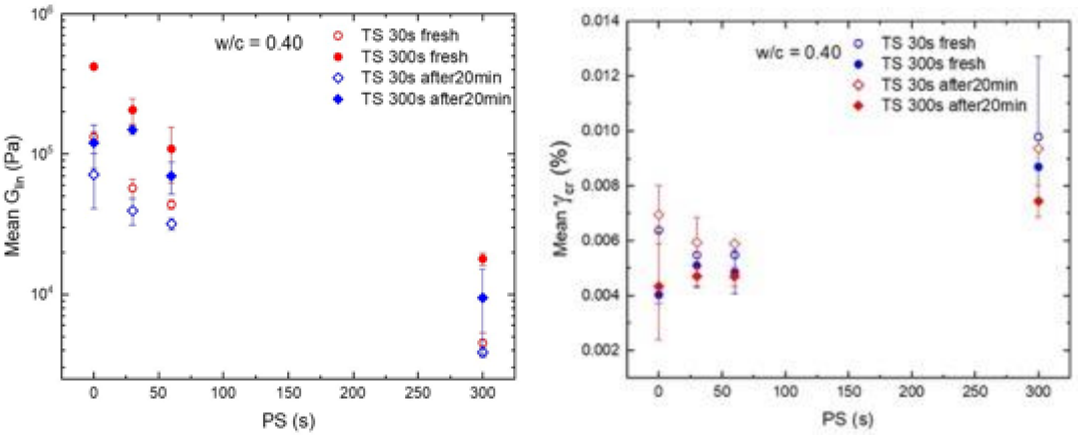

Fig. 3.8: Mean linear storage modulus, G'_{lin} (left) and mean critical strain, γ_{cr} (right) as a function of oscillatory pre-shear, OPS time (γ = 100%). Red dots: fresh; and blue diamonds: after 20 min.

Control

A comparative study of TS1 and TS2 (w/c = 0.40) (results not shown here) shows that: (a) G′ decreases with increasing PS times, (b) G′ values for fresh cements are always higher than the corresponding values after 20 min, (c) G′ values in TS1 are higher as compared to ones the TS2. The data for w/c = 0.35 are not shown, but as expected, they show that the G′ for w/c = 0.35 is always higher than for 0.40.

Discussion

Preparation steps

The duration and type of PS have a significant effect on the growth of elastic modulus (G′) during TS1 (Fig. 3.6 and Fig. 3.7). The final value of G′ at the end of TS1 is lower for higher duration of OPS, whereas duration of RPS does not significantly impact G′ values. The phenomenon of the dependence of TS1 on PS duration is observed in a recent work by M. Thiedeitz et al. [8]. The authors describe how the PS is responsible for breaking the cement particle agglomerates. Although in the paper, the sample is sheared in an external shear device and then transferred to the rheometer, in our work, we try to analyze the in-situ effect of the type and time of pre-shear within the plates of the rheometer.

The rotational pre-shear (RPS) does not show an impact on the sample structuration rate (TS1). This can be due to: (a) an insufficient shear intensity or duration or (b) slippage between sample and top plate which does not break down the structure of the sample during shear (i.e, the sample is not actually pre-sheared). The hypothesis needs to be confirmed either by using different geometries in rotation (i.e. vane, helical) or performing optical studies (for wall slip).

Looking at the trend in Fig. 3.6 and Fig. 3.7, we observe that G′ values of fresh samples in TS1 is higher than the corresponding values after 20 min, for both RPS and OPS. It is well known [4,11] that, in the first minutes after mixing, both C-S-H and early-stage ettringite are formed, resulting in a G′ increase. In order to explain this difference between the value of elastic modulus in fresh and after 20 min cement, a detailed analysis of the hydrates forming in the first hour of cement hydration is needed.

Measuring step

As shown in Fig. 3.8, the averaged value of G′ in the plateau (G'_{lin}) depends on the PS duration: G'_{lin} decreases with increasing OPS duration. This underlines the importance of PS duration on the structural break down of the samples in the early stage of hydration. It is also seen that G′ values for fresh cement are higher than the corresponding values of after 20 minute samples. Further investigation on the chemistry needs to be made.
We also note that the critical strain γ_{cr} is almost constant for all the PS durations, except for PS = 300 s, where it slightly increases. The trends of both G′ and γ_{cr} are in agreement with the ones shown in Work Package 5 (Influence of cementitious material, chemistry and grain size on fresh properties). A similar fractal analysis can be made to have information about the microstructure and the deformation mechanism.

Control step (results not shown here)

TS2 has similar trend as TS1. It is evident that the structural regrowth is an intrinsic property of the cement samples. An equal or slightly lower value of TS2 is due to the break-down in the measurement step (AS), and some irreversible changes likely related to hydration reactions. The trend in TS2 has a strong dependency on the PS, as for TS1. Once again, the choice of PS duration is crucial for the next experimental steps.

Conclusion

This report focuses on the effect of pre-shear on the internal structure, strength and rheological properties of cement paste. Fresh and after 20 min cement samples (w/c = 0.35 and 0.40) were studied in a high precision rheometer.
We defined three steps as: (a) conditioning, (b) measuring and (c) control. The conditioning step (a) comprises two parts: pre-shear (PS) and time structuration (TS1). During PS, the internal structure of the cement suspension is broken down by applying shear. During time structuration phase (TS1), the pre-sheared sample regains its strength and the growth of elastic modulus (G′) is recorded as a function of time. Our results show that the rate of time structuration (phase TS1) depends highly on the duration of oscillatory pre-shear (OPS): the increase in elastic modulus during time structuration is greater for lower pre-shear duration. This tends to show that oscillatory pre-shear is very efficient in breaking down the network of cement particles. We also note that no steady state of ”de-structuration” seems to be reached after 300s of pre-shear time. On the contrary, the rotational PS did not bring any significant change to the growth of elastic modulus during TS1. This can be attributed to an insufficient structural breaking down (or ”de-structuration”) by the applied shear rate of 10 s^{-1}, or to the slippage between the top plate and the cement during PS.
The storage modulus (G′) values during time structuration have a direct dependence on the sample age. The fresh cement has always higher G′ values. This phenomenon needs to be explored more, especially to identify which early hydrates form.
In the measuring step (b), an increasing oscillatory shear amplitude is applied as a continuous ramp. At small strain amplitudes, a linear storage modulus and a critical strain are defined, respectively G′ and γ_{cr}, to characterize the rest behavior of cement pastes.

We found that G′ depends on pre-shear duration and time, as for TS. The linear elastic modulus G'_{lin} is higher for low w/c ratio, as expected, whereas the γ_{cr} values are almost constant with the PS duration.
In the control step (c), TS2 shows similar trends as TS1 and depends on PS duration.
Based on the results, we can conclude that the pre-shear time and type have a strong effect on the internal structure of the cement. Moreover, oscillatory rheology on fresh cement can give an essential contribution to understand the early hydration chemistry and inter-particle dynamics. Last, phenomena related to the development of highly heterogeneous shear rates (such as slip or shear banding) need to be watched and should be investigated further with local measurements, using optical and an ultrasonic velocimetry technique.

Perspectives

Based on the results we have obtained until now, we plan to continue our investigation and focus on:
(1) early hydration chemistry and impact on early irreversible rheological behavior, function of cement chemistry. Presently, we are using C3A-free cement, and we will study a cement which instead includes C3A. We are also planning to study the chemical composition of the cement samples in time using XRD (X-ray powder diffraction).
(2) investigate other w/c ratios with the same rheological protocol and
(3) introduce superplasticizers to characterize their contribution.

Collaboration

This project is carried out in collaboration with Prof. Sébastien Manneville (ENS Lyon), Prof. Catherine Barentin (UCBL, ILM Lyon), Dr. Thibaut Divoux (ENS Lyon), Dr. Maurizio Pietro Bellotto (Chemical Eng. Dept., Politecnico di Milano)

References

[1] W.-H. Shih, W. Y. Shih, S.-I. Kim, J. Liu and I. A. Aksay, Physical review A, 1990, 42, 4772.
[2] T. Liberto, M. Le Merrer, C. Barentin, M. Bellotto and J. Colombani, Soft Matter, 2017, 13, 2014–2023.
[3] F. Marchesini, R. Oliveira, H. Althoff and P. De Souza Mendes, Journal of Rheology, 2019, 63, 247–262.
[4] H. F. Taylor et al., Cement chemistry, Thomas Telford London, 1997, vol. 2.
[5] H. Jennings, Cement and Concrete Research, 2000, 30, 101–116.
[6] B. Jönsson, A. Nonat, C. Labbez, B. Cabane and H. Wennerström, Langmuir : the ACS journal of surfaces and colloids, 2005, 21, 9211– 21.
[7] F. Van Bockstaele, PhD thesis, 2011.
[8] M. Thiedeitz, I. Dressler, T. Kränkel, C. Gehlen and D. Lowke, Materials, 2020, 13.
[9] M. Eslami Pirharati, H.-W. Krauss, C. Schilde and D. Lowke, Materials, 2020, 13, 2035.
[10] N. Roussel, G. Ovarlez, S. Garrault and C. Brumaud, Cement and Concrete Research, 2012, 42, 148–157.
[11] A. Zingg, L. Holzer, A. Kaech, F. Winnefeld, J. Pakusch, S. Becker andL. Gauckler, Cement Concrete Research, 2008, 38, 522 – 529.

WORK PACKAGE 4
Investigation of the influence of the mixing process

Introduction: Problem at stake

Ultra-High-Performance-Concretes (UHPC) are limited in their applicability not only due to their high cost (high solid content and additives) but also due to the type of mixers required to prepare them, and the energy cost associated with the mixing: intensive mixers such as Eirich mixers are powerful but expensive, and offer limited benefit when preparing ordinary concretes.

An alternative for the construction industry is to prepare UHPCs using dry pre-mixes and conventional mixers for the wet mix. In that case, the dry pre-mix needs to be sufficiently homogeneous (particles well dispersed) so that a conventional mixer would be sufficient to get the expected properties, both in fluid and solid states.

Typical water-to-binder ratio (w/b) for UHPC ranges between 0.14 and 0.20 [Shi et al, 2015], unlike conventional concretes where water-to-binder ratio is typically much higher, 0.4-0.5. This low water content is achievable though the use of superplasticizer, but also through maximum packing of particles, so that the amount of water that needs to fill the voids is minimal. This maximum packing is achieved through apollonian packing [De Larrard and Sedran, 1994]. The smallest particle added is typically silica fume, an industrial byproduct from ferro-silicium alloys production, with a size around 150 nm.

Intensive mixing is hypothetically needed in UHPC for two reasons: 1) Distribute water on the surface of all particles [Reschke et al, 2000], 2) Break the agglomerates of particles. Indeed, the nano-particles, due their high surface area, have strong interaction forces, and are especially difficult to break apart [Garrecht et al, 2010].

The questions we aimed at answering here are: What is the optimum dry pre-mix process, using a high intensity mixer, to reach optimal concrete properties, after wet-mixing in a conventional mixer? Do we confirm that breaking the agglomerated of nano-particles is the limiting step? Are mechanical properties of resulting UHPCs up to expectation?

In this project, we show that the main challenge during UHPC dry-mixing is indeed to break down the nano-particle agglomerates of silica fume, and that dry-pre-mixing followed by conventional wet-mixing offers a sustainable alternative for making UHPCs.

Material, Test Campaign & Procedure

Materials:

Cement ≈ 700 kg per cubic meter of mix (particle size D_{50} ≈ 15 μm)
Quartz powder ≈ 350 kg per cubic meter of mix (particle size ≈ 5-30 μm)
Silica fume ≈ 175 kg per cubic meter of mix (around 7 vol %) (particle size D_{50} ≈ 0.15 μm)
Sand ≈ 1000 kg per cubic meter of mix (particle size ≈ 100-500 μm)
Liquid / cement = 0.28
Superplasticizer ≈ 4.5 % by weight of cement (bwoc)
Consistency keeper ≈ 2.5 % by weight of cement (bwoc)

Mixing procedure:

- Mix all dry ingredients in high energy Eirich mixer (R08) for various amounts of time (between 0 and 480 min). Dry mixes were also stored for various amounts of time (few hours to 9 weeks), at room temperature.

- Wet mixing in a conventional Hobart mixer (450 W, 4 kg maximum) for 10 min or more, or in high energy Eirich mixer (R02) (4 kW, 10 kg maximum) for around 2 min.

Samples for strength measurement were molded and stored for 24 hours, and then further cured in ambient conditions for the remaining days before testing.

<u>Testing campaign</u>:

- Measurement of rheological properties using V-funnel cone (DIN EN 12350-9:), spread (DIN EN 12350-5) and a viscosimeter Viskomat NT from Schleibinger (following [Mazanec, 2012]).
- Measurement of set mechanical properties (compressive strength) following ÖNORM EN 196-1 on samples 40 x 40 x 40 mm^3 and using Toni Technik 3000 KN machine.
- Particle size distribution using a Mastersizer 3000 instrument from Malvern.

Results

- Influence of mixer type on compressive strength (28 D)

Solid samples obtained from wet mixes using an Eirich mixer R02 (green data) or a Hobart mixer (blue data) were tested. The dry pre-mixes were previously mixed with Eirich mixer R08 (dry mixing time between 1.5 min and 480 min).

Results on Fig. 4.1 show that UHPCs wet-mixed with high intensity Eirich mixer exhibit consistently higher strength (149 MPa on average). Nevertheless, wet mixes mixed with conventional mixers show good strength development, with an average at 144 MPa, a decrease of ≈ 4% on average.

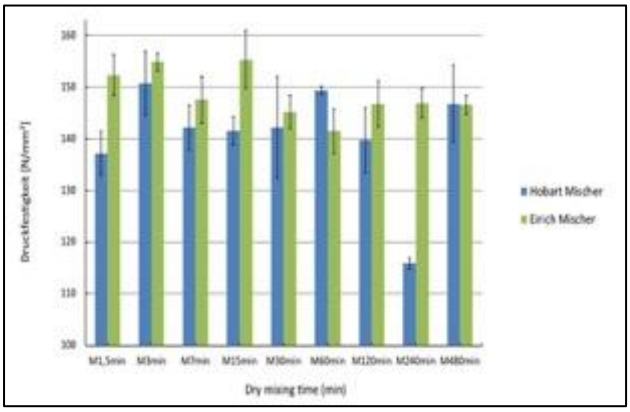

Fig. 4.1 – 28-day compressive strength plotted as a function of dry mixing time. Dry premixes were mixed with Eirich mixer R08 (dry mixing time between 1.5 min and 480 min) and wet mixes with Eirich mixer R02 (green data) or with Hobart mixer (blue data).

- Influence of dry mixing time on wet mixing energies

The power consumption was recorded during wet mixing, using the Eirich R02, because of its ability to capture this data. Results plotted Fig. 4.2 show that for the dry pre-mixing times of 1200 s (20 min) and 2400 s (40 min), the peak power was lower, and occurred sooner. This means that the wetting of the particles occurred faster and was easier when using a larger dry pre-mix duration.

The wet mixing energy was calculated by integrating the curve (right axis in Fig 4.2). It is respectively 65 kJ for a pre-mix that was dry-mixed for 1.5 min, 52 kJ for a pre-mix that was dry-mixed for 20 min (a 21 % decrease) and 44 kJ for a pre-mix that was dry-mixed for 40 min (a 33 % decrease).

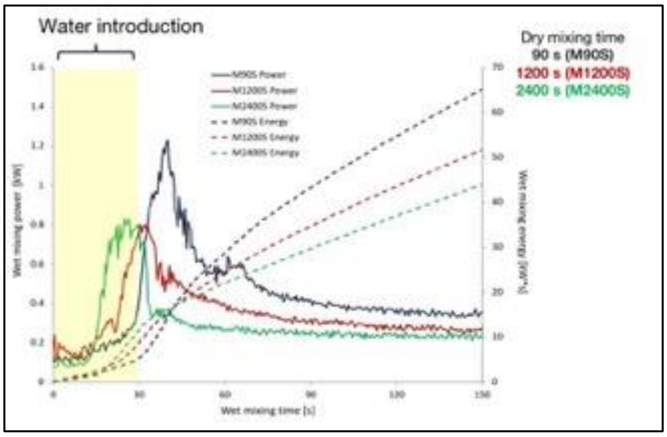

Fig. 4.2 – Wet mixing power and energy (using Eirich R02 mixer) function of mixing time for 3 different pre-mixes. Dry pre-mixes were mixed with Eirich mixer for 1.5 min (black), 20 min (red) and 40 min (green).

- **Influence of dry mixing time on rheology**

The rheology of the wet mixes was assessed using V-funnel cone and spread. Results plotted Fig. 4.3 show that the cone flow time (indicative of viscosity) drops from 64 s for zero dry mixing time to 10 s for 20 min dry mixing time, a 84 % drop. On the other side, the spread increases from 23 cm to 30 cm, a 31 % increase (indicating a decrease in yield stress).

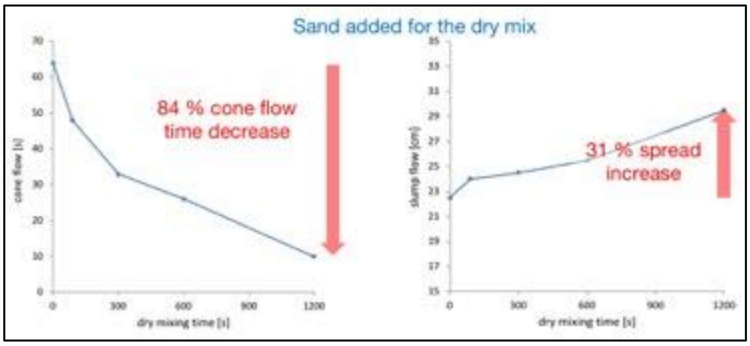

Fig. 4.3 – V-funnel time (left) and spread (slump flow) (right) of wet mixes (with sand added during the dry mixing phase) function of dry pre-mixing time.

- **Influence of presence of sand during dry mixing**

Sand is typically assumed to help break down agglomerates during the high intensity mixing step. Here, we compare the rheological properties (V-funnel time and flow spread) of the mixes when sand was added during the dry mix versus when sand was added during the wet mix, both using high intensity mixing. Results displayed Fig. 4.4. show that when sand is added later, i.e. during the wet mix, all points are shifted towards higher viscosity (longer funnel time) and higher yield stress (lower spread). Lower viscosity and yield stress tend to associate with broken agglomerates, although this is not a direct proof. This tends to show that sand may indeed help homogenizing the mix and break down silica fum

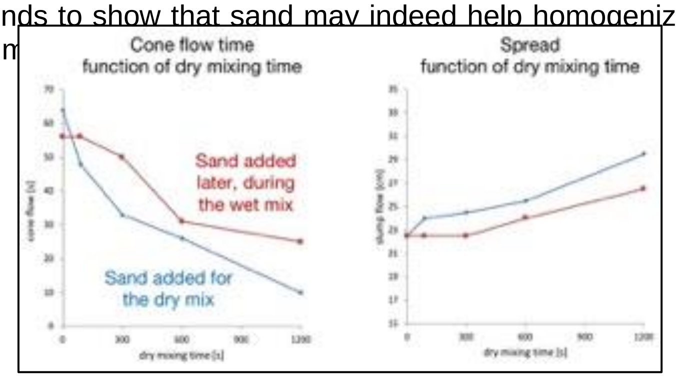

Fig. 4.4 – V-funnel time (left) and spread (slump flow) (right) of wet mixes with sand added during the dry mixing phase (blue) and with sand added during the wet mix (red) function of dry pre-mixing time.

- **Influence of dry mixing time on strength**

Compressive strength was measured on samples at 24 hours, 7 days and 28 days. Results plotted Fig. 4.5 show that the compressive strength at 24 hours slightly decreases with dry mixing duration. On the opposite, the 7-day and 28-day strength increase with dry mixing duration, specifically by around 10% when dry mixing time increases from 1.5 min to 20 min.

We hypothesize that the 7-day and 28-day improvement in strength with longer dry mixing time is related to silica fume higher de-agglomeration state.

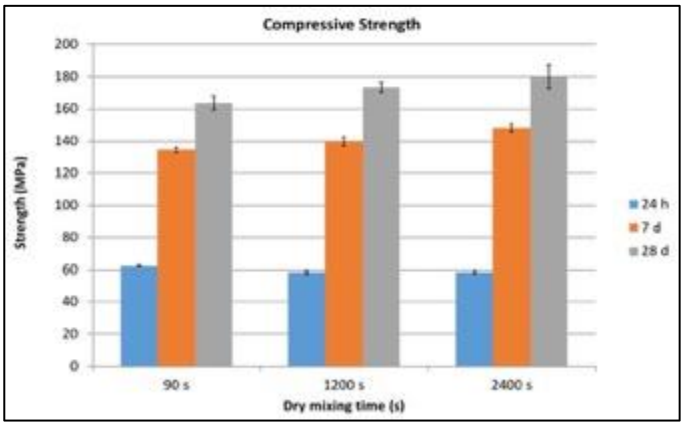

Fig. 4.5 – Compressive strength (blue, 1 day, orange, 7 days and grey, 28 days) for 3 pre-mix durations (90s, 20 min and 40 min). Half Error bar = (max-min)/2 for 3 samples each condition

- **Influence of dry mix shelf storage time on rheology**

The yield stress, viscosity and 28-day strength of mixes prepared using dry pre-mixes with varying pre-mix durations (between 1.5 min and 30 min) and storage time (3 days, 4 weeks and 9 weeks) were measured. Results, not shown here, show that dynamic yield stress, viscosity and 28-day strength look independent of the dry mix storage time, for mixes with longer (and appropriate) dry-mixing durations (7, 15 and 30 min).

- **Measurement of particle sizes in the mix, focusing on silica**

Fig. 4.6 shows a rough schematic of our understanding of the process of silica deagglomeration during the mixing process. Our understanding is that silica agglomerates traps water, that can then not be used for the mix. Because silica fumes have small individual particle sizes and high surface areas, we assume that the attractive forces are the strongest in the mix, and silica agglomerates are therefore the most difficult to break down during the mixing process [Garrecht & Baumert, 2010]. This leads us to think that measuring the size of silica particles (either agglomerates or single particles) may serve as a quality control for mix readiness: When a sufficient fraction of silica agglomerates is broken, we can consider the mix ready.

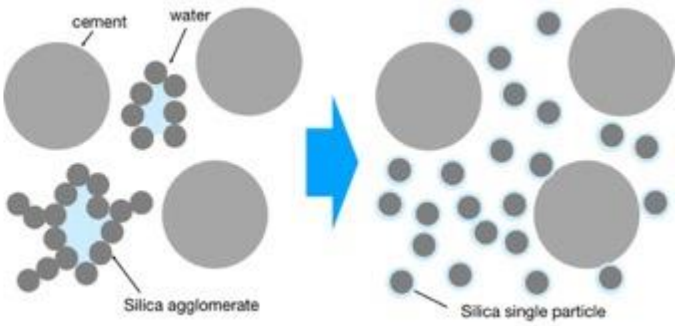

Fig. 4.6 – Schematic process of silica de-agglomeration during mixing process

The particle size distributions of the mixes were measured after various amounts of dry mixing times, between 1.5 min and 480 min. Results, shown Fig. 4.7, show a tri-modal particle size distribution, with peaks around 210 nm, 24 µm and 350 µm. These three sizes are assumed to respectively correspond to silica fume particles, cement and quartz grains, and sand grains. The y-axis plots the volume density of particle at a given size, and the latter does not exhibit any variation with dry mixing time. This result contradicts all other indirect measurements presented before, and that tended to show that silica was de-agglomerating and releasing water/superplasticizer with increasing dry-mixing duration: viscosity and yield stress of the wet mixes decrease with dry mixing time, or equivalently flow time increases and spread flow increases with dry mixing time. It is important to note that measuring four different components simultaneously on the Mastersizer instrument likely gives erroneous results. Indeed, each component/particle has its specific optical parameters (Refractive Index, RI, and Adsorption Index, AI), and these parameters need to be properly defined. For measuring a mixture made of different components, we applied average values of RI and AI of all particles, decreasing the accuracy of the results. Calculating the packing density (using Schwanda model) from these measurements gives, unfortunately, no satisfying results at this point.

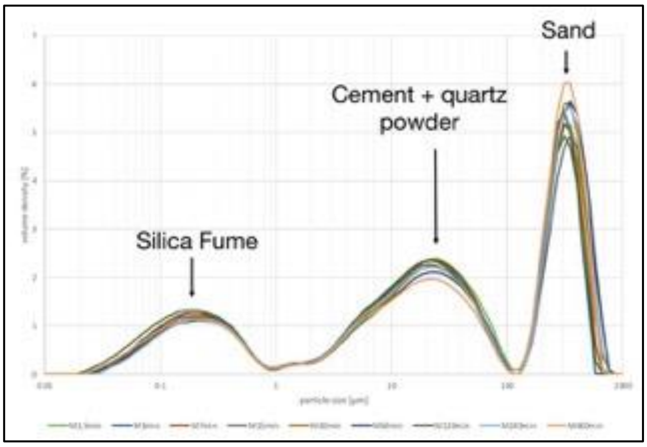

Fig. 4.7 – Particle size distribution of the complete mix for various amounts of dry mixing times.

Conclusion

The most important result of this work is that we show that a two-step mixing process (dry pre-mix using high intensity mixing, and wet mixing using a conventional mixer) produced UHPCs with good mechanical properties, comparable to properties obtained when mixing the UHPC with high intensity mixing only. Concretes that were wet mixed with a high intensity mixer show an average of 149 MPa strength, while these that were wet mixed with a conventional mixer exhibited strength only 4% smaller with an average at 144 MPa.

We also measured that increasing the dry pre-mixing duration from 1.5 to 20 minutes increased the 7-day and 28-day strength by 10% and reduced the energy necessary to wet-mix by 33%. It also decreased the cone flow time (V-Funnel) by more than 80% and increased the flow spread by 30%.

Finally, we measured that storage time (tested up to 9 weeks) does not degrade the dry-mix (not shown here).

All these results indirectly show that large de-agglomeration of particles occur during the dry mixing time and is beneficial to the concrete. The ultimate and direct proof would come from the measurement of particle size distribution, which at this point in the project could not discriminate between the mixes.

Literature

Reschke,T; Der Einfluss der Ganulometrie der Feinststoffe auf die Gefügeentwicklung und die Festigkeit von Beton, VBT, 2000

Garrecht, H; Baumert,Ch.: Mischen von Hochleistungbetonen. Beton- und Stahlbetonbau 105 (2010), Heft6

Shi C., Wu Z., Xiao J., Wang D., Huang Z., Fang Z., A review on ultra high performance concrete: Part I. Raw materials and mixture design, Construction and Building Materials, Volume 101, Part 1, 2015, Pages 741-751

Roussel N., Understanding the rheology of concrete, edited by Roussel, Woodhead publishing,

2012
de Larrard F. and Sedran T., Optimization of UHPC by the use of a packing model, Cement and Concrete Research, Vol. 24, No. 6, pp. 997-1009 (1994)
Mazanec O. J., Charakterisierung der Mischzeit und des rheologischen Verhaltens ultrahochfester Betone unter Einbeziehung interpartikulärer Wechselwirkungen, PhD Thesis, Technischen Universität München (2012)

WORK PACKAGE 5

Influence of cementitious material, chemistry and grain-size on fresh properties

Introduction

Alkali-activated binders have been widely discussed and promoted as an essential component of the current and future toolkit of ‘sustainable cementing binder systems’ [5]. However, when selecting a binder alternative to OPC, it is necessary to take into account several aspects beyond the mere mechanical performances and durability properties. First of all, if the binder is used to produce a ready-mixed concrete, it is advisable to use a “one part” material which sets and hardens upon contact with water only, so that the available mixing and processing technologies can be used [6]. Also, with regards to the life-cycle assessment (LCA), the impact of the activating system needs to be duly included. In the case of sodium hydroxide or sodium silicate activation, the LCA will be negatively and significantly impacted [7]. Finally, the fresh-state properties, the response to the addition of superplasticizers and the cohesivity and pumpability of AAB may widely differ from OPC. These requirements are sometimes conflicting with regards to the choice of the AAB system. In the following study, we selected a well-known and long-time used AAB constituted by ground and granulated blast-furnace slag (GGBS) activated with sodium carbonate (or sodium sulphate) [8]. A number of buildings erected with such a binder in the 1950s show little signs of degradation apart from carbonation and are still having compression strength higher than the design values [9]. This binder also has a low environmental footprint, good resistance to environmental attack and it is aesthetically alike to white cement. It is however less cohesive than OPC and does not respond properly to the addition of superplasticizers [10].

The control of cohesivity and the adsorption of superplasticizer are regulated by the surface charge density, surface potential, the ionic composition and ionic force of the interstitial solution [11]. In this study, we measure and compare the rheological properties of OPC and AAB with a model system, a calcite paste, that has been fully characterized in terms of macroscopic and microscopic behavior [3,4]. We interpret the rheological behavior of these suspensions in the framework of the classical fractal elasticity model proposed by Shih et al. [1], with an effort to relate the observed behaviour to the interparticle forces. Our goal is to develop a tool to interpret the role of the surface-solution equilibria in particle attraction and surface polymer adsorption potential.

Materials and methods

Samples preparation

An Ordinary Portland Cement CEM I 52.5 R powder (from Cementi Rossi, Italy, of picnometric density 3140 kg.m^{-3}) was mixed directly in distilled water with w/c ratio varying from 0.5 to 0.3 (corresponding to φ =0.39-0.51). The mixing was done with a vortex stirrer (Ultra Turrax TD300 from IKA) for three minutes at increasing rotation speed from 2800 rpm to 5800 rpm.

The alkali activated slurry (AAS) was obtained by dispersing GGBS (from Ecocem

France, with D50 = 11 μm and density of 2944 kg.m^{-3}) in distilled water adding sodium carbonate Na_2CO_3 (reagent grade from Sigma Aldrich, density 2540 kg.m^{-3}) as solid activator and calcium hydroxide $Ca(OH)_2$ (ventilated hydrated lime CL90-S from Unicalce, Italy, density 2211 kg.m^{-3}) as a setting and hardening accelerator. The binder formulation is: 91.5% of GGBS, 5% of Na_2CO_3 and 3.5% of $Ca(OH)_2$ (density 2891 kg.m^{-3}). The formulation involves stoichiometric amounts of Na_2CO_3 and $Ca(OH)_2$, to optimize both the early setting and the long-term strength [12]. The binder to water ratio is varied from 0.5 to 0.3 (corresponding to φ =0.41-0.53). The mixing process is analogous to the one of CEM I.

As detailed in [3], to obtain calcite dense colloidal suspensions, Socal 31 calcite powder (Imerys, average particle diameter 75 nm, density 2710 kg.m^{-3}) is also dispersed in distilled water. The maximum range of volume concentrations reached is φ = 5-30%. The mixing process was carried out in the same vortex stirrer for five minutes at an increasing mixing rate with the volume concentration from 2800 to 5800 rpm.

Rheological measurements

Rheological measurements were performed with a stress controlled rotational rheometer (Anton Paar, MCR 302). Oscillation tests were made with a plate-plate geometry (Anton Paar, PP50 and PP25) at room temperature (20 ± 0.5°C). Plates were either roughened (AAS and CEM I) or covered by sand paper (calcite), in order to avoid wall-slip together with an optimized gap for each system **[3]**. In particular, the gap is set to 2 mm for the CEM I and the AAS and 4 mm for the calcite paste. A moisture chamber was also used to avoid evaporation, particularly significant in the case of AAS. The “oscillation protocol” is constituted by: (i) a one-minute pre-shear at imposed shear rate of 10 s^{-1} (or deformation γ = 10 %) in which the sample shear stress history is reset, (ii) a time structuration step at low deformation, in the range of elasticity of each system (γ = 0.0005% and t = 2 min for CEM I and AAS - γ = 0.01 % and t = 5 min for calcite) and frequency 1 Hz in which the sample reaches a pseudo-steady state, increasing the elastic storage modulus G’ and reaching a plateau after 1-2 minutes and (iii) an amplitude sweep at the imposed frequency of 1 Hz with increasing deformation from 0.0001 to 10%. The measurements were performed at different volume concentrations, to explore the variation of the elastic properties. As detailed in **[3]**, we extracted a linear storage modulus, G'_{lin} (i.e. storage modulus in the linear regime at low deformation), and a critical strain, γ_{cr} (i.e. value of deformation at the end of the G’ linearity), and we compare the different behavior of the three systems as discussed below.

Results

Fig. 5.1 and 5.2 show the influence of the volume fraction φ on the elasticity parameters G'_{lin} and γ_{cr} for the three systems.

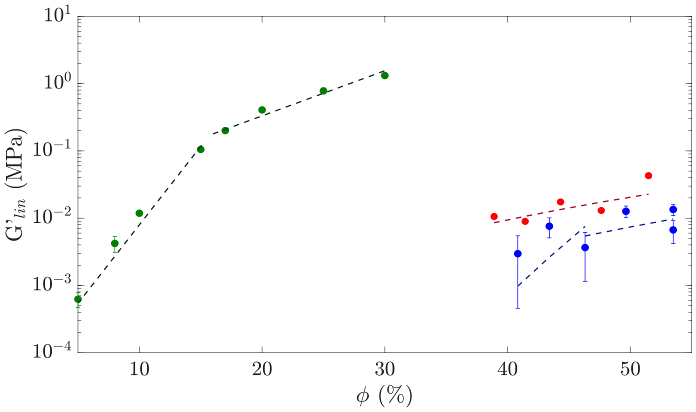

Fig. 5.1: Linear storage modulus G’$_{lin}$ as a function of the volume concentration φ for the three suspensions: calcite (green points), CEM I (red points) and AAS (blue points). The dashed lines represent the plot of the scaling model proposed by Shih et al. [1] as described in the discussion section. Error bars indicate the reproducibility of the results. Notice that the y-axis is in a logarithmic scale.

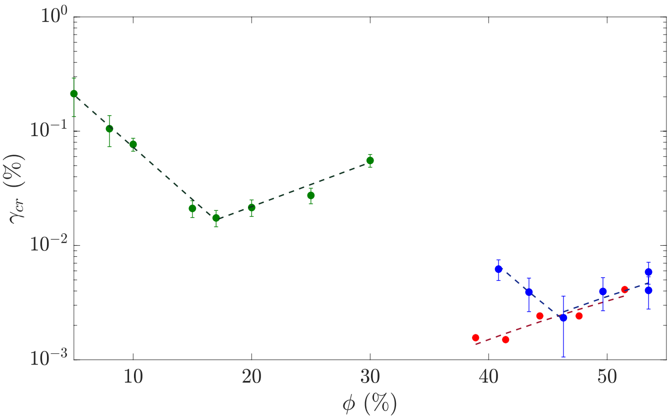

Fig. 5.2: Critical strain γ$_{cr}$ as a function of the volume concentration φ for the three suspensions: calcite (green points), CEM I (red points) and AAS (blue points). The dashed lines represent the plot of the scaling model proposed by Shih et al. [1] as described in the discussion section. Error bars indicate the reproducibility of the results. Notice that the y-axis is in a logarithmic scale.

Starting with calcite, G’$_{lin}$ constantly rises when φ increases, with a slope change around φ = 17%. This non-monotonic trend is strongly confirmed by the γ$_{cr}$ that shows a two-slope scaling behavior **[3]**.

Both CEM I and AAS systems are shifted at a higher volume concentration range corresponding to a water to binder ratio between 0.5 and 0.3. This shift is mainly due to the different particle size and the nature of the interparticle interaction, as detailed in the discussion section.

Looking at both systems in Fig. 5.1, they seem to have a similar behavior. In Fig. 5.2 instead, CEM I shows a γ$_{cr}$ which increases monotonically, while the AAS presents the same two-slope behavior observed for calcite.

Discussion

The amplitude sweeps have been measured, for each system, in the volume concentration range where the system has a gel-like behavior. The system can flow under shear, with isolated flocs (clusters of particles) dispersed in the continuous interstitial solution, while at rest can form a continuous path of solid particles across the entire volume, which causes the appearance of elastic behavior with G’>G”. We describe the elastic response to the small amplitude deformations according to a classical fractal model proposed by Shih et al. **[1]**. This model was originally proposed for colloidal suspensions such as our calcite paste, but it can be extended to all systems whose behavior is controlled by colloidal surface forces, even if the particle dimensions are outside the Brownian motion regime **[2]**.

The structure of the gel network is considered as constituted by fractal flocs (i.e. “repetitive highly porous aggregate composed of smaller primary particles” **[13]**). The rigidity and the deformation mechanism depend on the density and structure of the flocs, both function of the interaction forces between the particles **[14]**. Moreover, Shih et al. **[1]** define two regimes which depend on the compactness of the particle network (i.e. fractal dimension d_f) and which give rise to different trends of G'_{lin} and γ_{cr} as a function of φ (Fig. 5.1 and 5.2). At low φ, the floc is porous and deformable under shear. The bond between different flocs is strong compared to the intra-floc bonds, so that the weakest elements are the links between the particles inside the flocs. At high φ instead, the flocs are dense and rigid, and the deformation under strain occurs between different flocs. The power law scaling of the elastic modulus and critical strain are: (1) $G'_{lin} \propto \varphi^A$, (2) $\gamma_{cr} \propto \varphi^B$. Analogously the same equations can be extracted for a critical stress τ_{cr}, resulting from the product of G'_{lin} and γ_{cr}: (3) $\tau_{cr} \propto \varphi^C$, where C is the sum of A and B. The scaling exponents are presented in Table 1 directly for the two regimes, respectively deformable and rigid flocs (DF and RF). The detailed derivation of these exponent is explained extensively in **[1, 2]**.

Tab. 5.1: *Exponent of the power law for G'_{lin} and γ_{cr} as a function of the fractal dimension d_f for the different regimes (i.e. DF, Deformable Floc and RF, Rigid Floc).*

	DF	**RF**
A ($G'_{lin} \propto \phi^A$)	$4/(3-d_f)$	$1/(3-d_f)$
B ($\gamma_{cr} \propto \phi^B$)	$-2/(3-d_f)$	$1/(3-d_f)$
C ($\tau_{cr} \propto \phi^C$)	$2/(3-d_f)$	$2/(3-d_f)$

As shown in Tab. 5.1, the slope of the exponent is always positive, except for γ_{cr} in the deformable regime. This can be observed in Fig. 5.2 for the calcite and AAS at lower φ in the respective volume concentration range. From the scaling laws of G'_{lin}, γ_{cr}, τ_{cr} as a function of φ, the fractal dimensions d_f are calculated and reported in Tab. 5.2 for the three systems at rest (i.e. small amplitude oscillation measurements). We expected that, under shear (i.e. flow measurements), the continuous, percolated structure formed at rest is destroyed, forming isolated rigid flocs with a resulting floc fractal dimension closer to 3.

Tab. 5.2: *Fractal dimension d_f calculated for the three different systems in the two different regimes (i.e. DF, Deformable Floc and RF, Rigid Floc).*

	d_f **(DF)**	d_f **(RF)**
CEM I	-	2.71
AAS	2.73	2.75
$CaCO_3$	2.23	2.61

We can notice that for both calcite and AAS suspensions, both regimes are present. As extensively discussed in **[2]**, the presence of both regimes, when exploring the influence of volume fraction only (i.e. no external forces), is not common in colloidal systems and it is surprising to find it also in a non-colloidal one (i.e. AAS). This behavior for our AAS is the sign of weak inter-particle interactions and flocs which become stiffer when growing larger.

Differently, CEM I, despite the similarity with AAS in the high concentrated paste condition state, is presenting only the rigid floc regime throughout the range of φ. Before going into detail about the nature of the three different systems, the different deformation mechanisms are schematically illustrated according to the Shih et al. **[1]** scaling fractal model in Fig. 5.3.

In particular, if we compare Fig. 5.2 with Fig. 5.3, we can recognize the regime of floc deformation (a_1 to a_3, b_1 to b_3) and the regime of rigid flocs (a_2 to a_4, b_2 to b_4, c_1 to c_3, c_2 to c_4).

The different deformation regimes determine microstructural differences of the three systems. The calcite used in this study is a nano-powder which creates, once suspended with water, weak electrostatic attraction between particles. The nature of these interaction (DLVO) was fully described (as detailed in **[3]**) thanks to the study of the rheology and the physico-chemistry of the suspensions.

Systems like CEM I and AAS are constituted by micrometric particles and, when suspended in water, interact via short-ranged electrostatic and correlation forces that produce short distance electrostatic forces **[11]**. This explains the narrower volume fraction range at which an CEM I and AAS elastic pastes are formed and which are really sensitive to the complex chemistry of the solution.

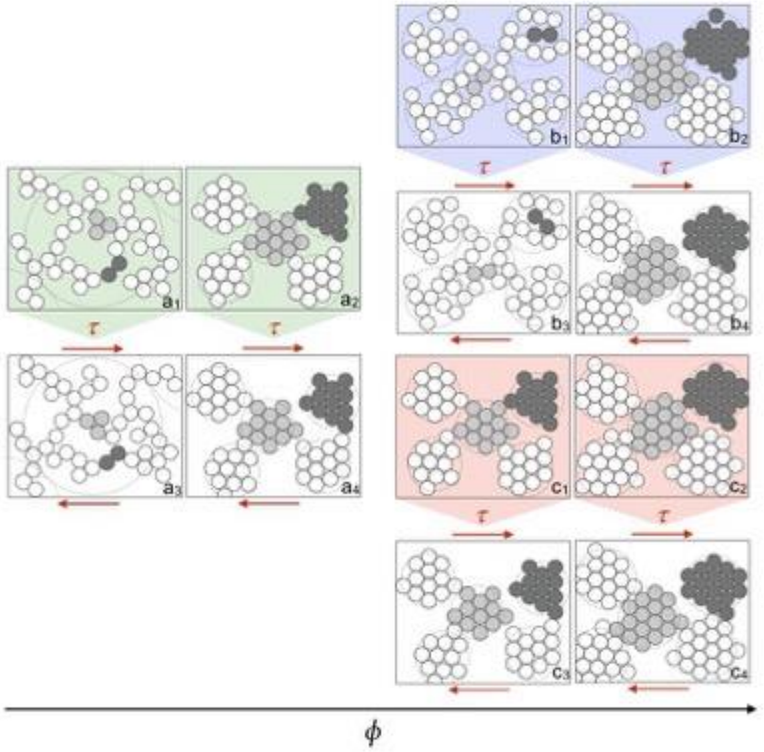

Fig. 5.3: Schematic floc deformation mechanism at different volume concentration φ for the three systems: calcite (a1-a4), AAS (b1-b4) and CEM I (c1-c4). The dashed lines represent the floc. The upper part of each system (light colored) represents flocs at rest and the lower part the new floc configuration after imposing a deformation. Few particles or flocs are colored (i.e. light or dark grey) to help visualize the floc reconfiguration through the movement of the individual particles.

Conclusion & Perspective

The observed differences between the rheology of cement and AAS illustrate the different cohesivities of the two pastes. We show on this study that rheology is an important tool to investigate the paste cohesivity, deformation and flow mechanisms, and surface properties. In a follow-up study, we plan to investigate the rheology of the two systems in the presence of superplasticizers, and aim at elucidating the reason behind the high effectiveness of common superplasticizers on cement but not on alkali activated materials.

Bibliography

[1] Shih, W.-H., Shih, W. Y., Kim, S.-I., Liu, J. and Aksay, I. A.: Scaling behavior of the elastic properties of colloidal gels. Physical Review A, 1990.
[2] Bellotto, M.: Cement paste prior to setting: A rheological approach. Cement and Concrete Research, 2013
[3] Liberto, T., Le Merrer, M., Barentin, C., Bellotto, M., and Colombani, J.: Elasticity and yielding of a calcite paste: scaling laws in a dense colloidal suspension. Soft Matter, 2017.
[4] Liberto, T., Barentin, C., Bellotto, M., Colombani, J., Costa, A., Gardini, D. and Le Merrer, M: Simple ions control the elasticity of calcite gels via interparticle forces. Journal of Colloid and Interface Science 2019.
[5] Shi, C., Roy, D. and Krivenko, P., Alkali-activated Cements and Concretes. Taylor & Francis, 2006.
[6] Luukkonen, T., Abdollahnejad, Z., Yliniemi, J., Kinnunen, P. and & Illikainen, M.: One-part alkali-activated materials: A review. Cement and Concrete Research, 2017.
[7] Habert, G., d'Espinose de Lacaillerie, J.B. and Roussel, N. : An environmental evaluation of geopolymer based concrete production: reviewing current research trends. Journal of Cleaner Production, 2011
[8] Purdon, A. O.: Improvements in processes of manufacturing cement, mortars and concretes. British Patent GB427227A, 1935.
[9] Buchwald, A., Vanooteghem, M., Gruyaert, E., Hilbig, H., and De Belie N: Purdocement: application of alkali-activated slag cement in Belgium in the 1950s. Materials and Structures, 2015.
[10] Palacios M., Houst Y.F., Bowen P. and Puertas F.: Adsorption of superplasticizer admixtures on alkali-activated slag pastes. Cement and Concrete Results, 2009.
[11] Jönsson, B., Nonat, A., Labbez, C., Cabane, B. and Wennerström, H.: Controlling the Cohesion of Cement Paste. Langmuir, 2005.
[12] Bellotto M., Dalconi M.C., Contessi S., Garbin E. and Artioli G.: Formulation, performance, hydration and rheological behavior of 'just add water' slag-based binders. Proceedings of the 1st International Conference on Innovation in Low-Carbon Cement and Concrete Technology, London 2019.
[13] Jarvis, P., Jefferson, B. and Parsons, S. A.: Measuring Floc Structural Characteristics. Reviews in Environmental Science and Bio/Technology, 2005.
[14] Shih, W.Y., Shih, W.H. and Aksay, I.A.: Elastic and yield behavior of strongly flocculated colloids. Journal of the American Ceramic Society, 1999.

WORK PACKAGE 6

Characterization of the concrete-to-concrete interface: experimental evaluation of temperature effect on epoxy interfacial bond strength

Introduction

Nowadays, multi-layered concrete composites have been increasingly used in a wide range of applications such as buildings, bridges, roads, and dams. Using precast members in new structures and strengthening/repairing the existing structures are among the main reasons for employing these composites (D. S. Santos et al., 2012). Depending on the application, a hardened or a fresh concrete can be placed against a hardened concrete substrate layer, such as the precast parts in bridge decks and concrete overlays in repaired structures (Emmons, 1994; P. M. D. Santos, 2010; Silfwerbrand, 1990).

Due to the material discontinuity, high pore accumulation, and micro-crack concentration, the concrete-concrete interface is treated as a weak point and critical area within the composite (Emmons, 1994; He et al., 2017). Relative slippage, debonding and delamination are among the most common problems indicating a non-monolithic behavior (P. M. D. Santos & Júlio, 2013; Zanotti & Randl, 2019). Therefore, a well-designed multi-layered composite should present a strong interfacial bond to sufficiently transfer the load between concrete parts and hence achieving a monolithic behavior.

The concrete-to-concrete interface is a place of interest for researchers because it does not only play a key role on the durability and monolithic behavior of the composite, but it is also affected by numerous factors and has to be optimized. Therefore, the research efforts on the concrete-concrete interface have mainly focused on the improvement and assessment of the bonding (Júlio et al., 2006; Li, 2003; Zhang et al., 2020). The durability, performance, and bond strength of the interface have been investigated by the means of various test methods developed for this purpose. Although each of these test methods uses different specific configurations, the stress state at the interface is the main difference among them. Due to these differences, the bond strength value is highly dependent on the type of test method. As shown by (Momayez et al., 2005), the bond strength value gained by some test methods were greater up to 8 times compared to that of other test methods for the same specimens. Thus, evaluating the bond strength based on the results of one test method only can give misleading information. Therefore, our choice was to use three different methods.

Many studies have been carried out to assess the influence of various parameters on the multi-layered composite bonding. However, the effect of temperature (pre-conditioning and early-stage curing) on the concrete-concrete bond strength has not been fully investigated so far. Our hypothesis is that controlling the temperature will lead to better bonding and increase the interfacial bond strength. To check this, our work investigated the effect of temperature on the interfacial bond strength. To draw a reliable conclusion irrespective of the specific test method, three different test methods were employed and the interface performance was investigated under different temperatures.

Materials and methods

Concrete mixture

In this research, two different types of concrete, C30/37 and C45/55, were used to cast the substrate layer. In real applications, the overlay concrete has lower strength, due to its younger age. To take this differential strength into account in our lab experiment, the weaker concrete type of C30/37 was employed for the overlay layer. The properties of the concrete mixtures are presented in Tab. 6.1. All concrete mixtures were prepared with the same *contragress CEM I 42.5 N* cement.

Tab. 6.1 Mix proportions of substrate and overlay layers

Layer	Cement (kg/m^3)	Water (kg/m^3)	W/C	Fine aggregate [0-4 mm] (kg/m^3)	Coarse aggregate [4-16 mm] (kg/m^3)
Substrate I (C30/37)	300	180	0.6	860.7	1052
Substrate II (C45/55)	315	157.5	0.5	882.3	1078.5
Overlay (C30/37)	300	180	0.6	860.7	1052

Composite preparation procedure

To assess the effect of temperature on the interfacial bond strength in a wide range of applications, six different temperature values, namely 5, 15, 25, 35, 45, 55 ºC, were investigated. For each temperature value, a composite plate specimen (50×25×6 cm^3) was prepared as shown in Fig. 6.1. The preparation procedure employed for each composite is described below.

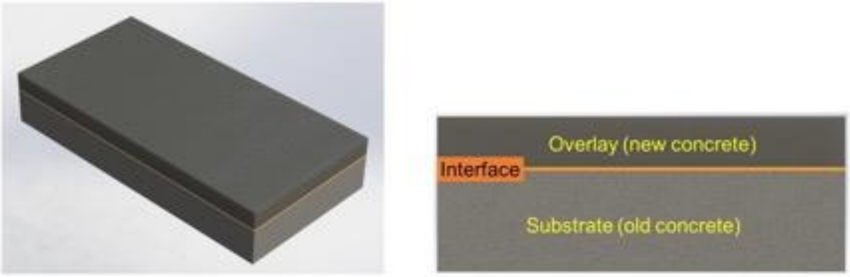

(a) (b)

*Fig. 6.1 - Schematic of composite plate specimen; **(a)** 3D model, **(b)** cross section*

In the first step, the substrate layer with dimensions of 50×25×6 cm^3 was cast and then cured for at least 28 days in the lab ambient environmental conditions. To prepare the surface of the substrate layer (roughness), the shot blasting method was employed. As depicted in Fig. 6.2, shot blasting is a one-step surface treatment method in which tiny steel shots are directed at high velocity against the concrete surface, resulting in removing contaminants, profiling, and roughening the concrete surface all at once.

(a) **(b)** **(c)**

*Fig. 6.2 - Surface treatment; **(a)** shot blasting **(b)** steel shots **(c)** prepared roughened surface*

The temperature effect was induced in two stages: (1) Pre-conditioning and (2) Early stage curing. For pre-conditioning, the cured substrate layer as well as all the components of concrete overlay (aggregate, cement, water) and epoxy bonding agent (resin, hardener, and sand quartz) were put in the climate chamber adjusted to the mentioned temperature values and kept there for 24 hours without humidity control.

The overlay components were then taken out of the climate chamber and mix together for 3 minutes. The epoxy components were also taken out and mixed as shown in Fig. 6.3. Quartz sand was added to the mixture of resin and hardener to prevent the penetration of the bonding agent into the depth of the substrate layer. The ratio of quartz sand to the resin to hardener was 4.7:3.7:1. The epoxy was then applied and spread on the substrate layer using epoxy roller.

Tab. 6.2 - Epoxy characteristics

Product description	MasterTop P 604 (two-component epoxy resin-based primer)	
Density (at 23 ºC)	Part A (resin)	1.62 g/cm^3
	Part B (hardener)	1.02 g/cm^3
	Mixed	1.44 g/cm^3
Viscosity (at 20 ºC)	Part A (resin)	9500 mPa.s
	Part B (hardener)	80 mPa.s
	Mixed	1400 mPa.s
Compressive strength (after 28 days)		55 N/mm^2
Tensile strength (after 7 days)		10 N/mm^2
Shore D hardness (after 7 days)		79

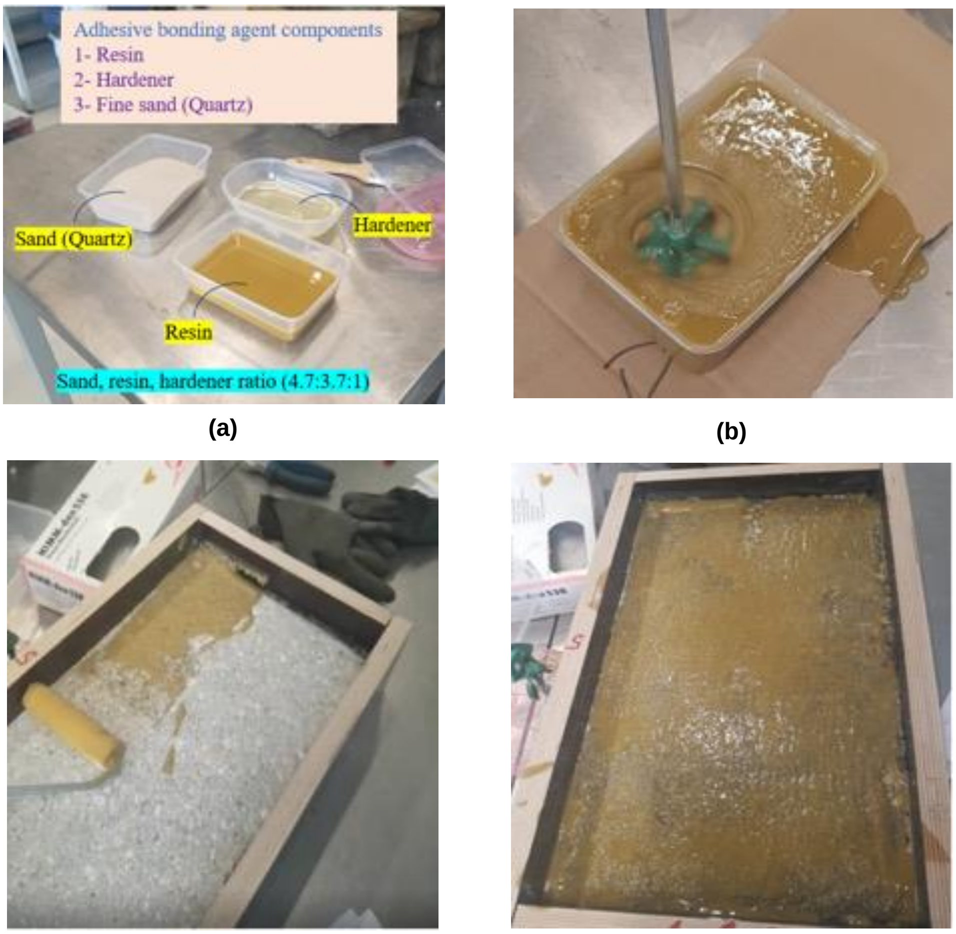

(a) **(b)**

(c) **(d)**

*Fig. 6.3 - Epoxy bonding agent; **(a)** components, **(b)** mixing, **(c)** spreading **(d)** prepared interface*

In the next step, the concrete overlay mixture was immediately placed on top of the epoxy, reaching a thickness of 3 cm. The composite specimen was then returned to the climate chamber adjusted to the given temperature for 7 days. The main purpose was to consider the effect of temperature in the early-stage curing process in addition to the pre-conditioning and understand how the temperature will affect epoxy curing, concrete setting, and their interaction. After 7 days, all the composite specimens were taken out from the climate chambers and cured in the lab ambient environmental conditions for at least 21 days.

Test methods

In this study, three different types of experimental test methods were used to assess the interfacial bond strength under various types of stress state at the interface, namely pull-off, wedge splitting, and bi-surface tests.

The **pull-off** is a method used to measure the tensile bond strength directly. In this method, a core is drilled through the overlay into a specific depth (15-20 mm) within the concrete substrate. As shown in Fig. 6.4, the pulling force is applied through a steel disc glued on the upper surface of the core allowing to pull on the core with a force that is perpendicular to the interface. Due to its simplicity, the test can be used for both laboratory and in-situ assessment and is therefore recommended by many standard codes.

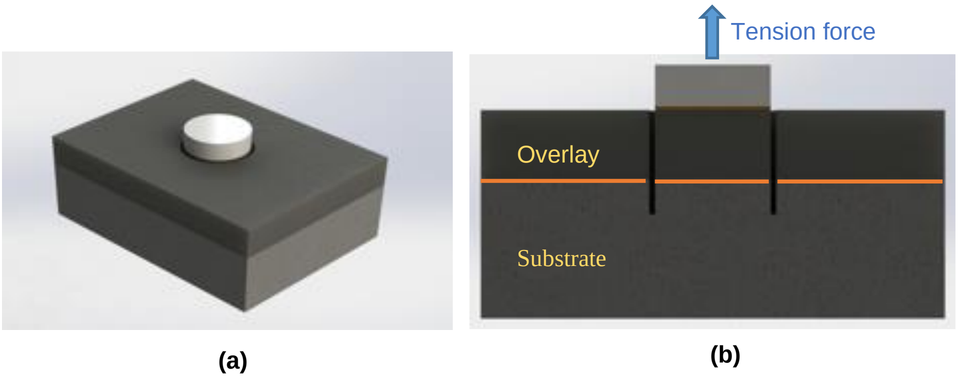

(a) **(b)**

Fig. 6.4 - Pull-off test setup; ***(a)*** *3D model* ***(b)*** *cross section*

In this work, all the cores were 5 cm in diameter and core boring was done with the penetration depth of 2 cm into the substrate layer giving a total core height of 5 cm (Fig. 6.5). The steel dollies were then glued to the surface of the cores and after 24 hours of curing, the pulling test was done. The monotonic tension loading was applied with the rate of 50 N/s by the means of *Proceq* pull-off tester. The interfacial tensile strength was calculated using the measured value of failure tensile force and the surface area of the core (19.63 cm^2).

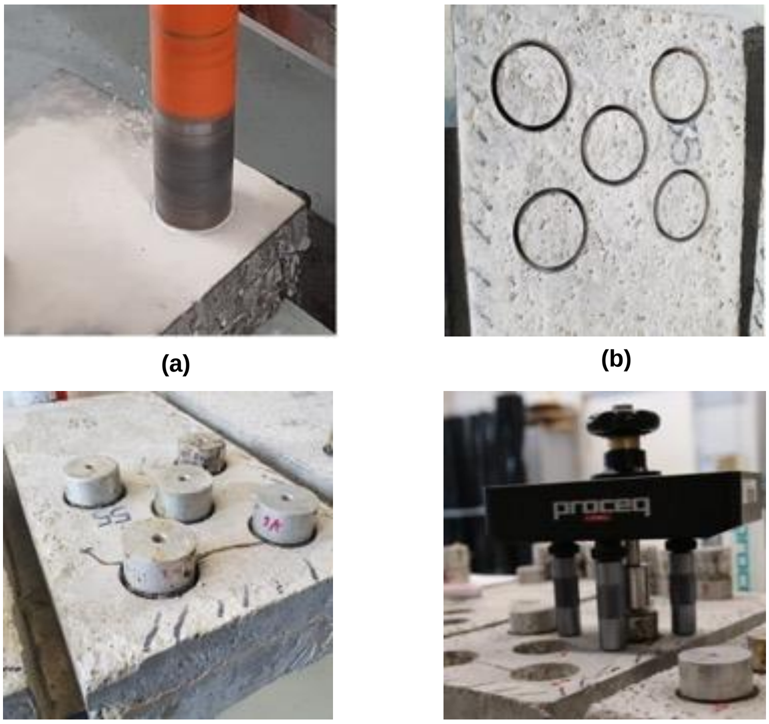

(a) (b) (c) (d)

Fig. 6.5 - Pull-off test experiment; ***(a)*** *core boring,* ***(b)*** *cores,* ***(c)*** *glued steel dollies,* ***(d)*** *pull-off tester*

The **wedge splitting test (WST)** was originally introduced by (Linsbauer & Tschegg, 1986) and was further refined by (Brühwiler & Wittmann, 1990). This method is usually used to evaluate the crack opening Mode (Mode I) and subsequently the fracture properties, e.g. the fracture energy and softening diagram of the quasi-brittle materials, such as concrete. As shown in Fig. 6.6, the stiff wedge is subjected to the compressive force on the upper part of the specimen and by the means of roller bearings, the vertical compressive load will be converted to horizontal loads, eventually splitting the specimen into two parts.

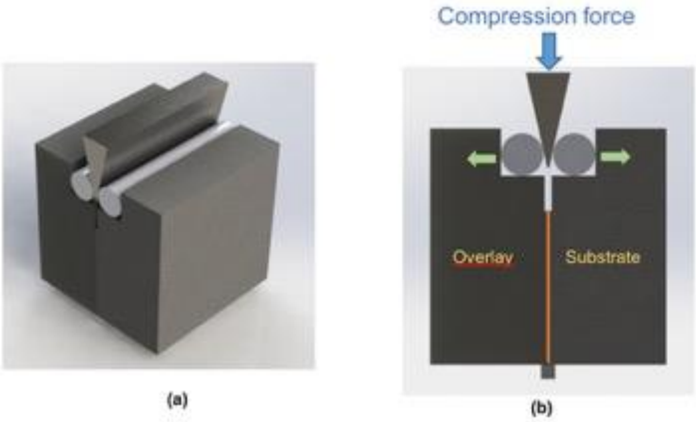

Fig. 6.6 - Wedge splitting test setup; ***(a)*** *3D model* ***(b)*** *cross section*

In this study, four replicate samples were cut from each composite. The WST samples were 10×9×8 cm^3 prisms, and a notch of depth 2 cm was sawed exactly along the interface. The samples were then subjected to the compressive loading with a monotonic vertical displacement rate of 0.2 mm/s by the means of Zwick 250 kN loading machine.

Fig. 6.7 - Wedge splitting test (WST) experiment

The vertical compressive load (F_v) and crack mouth opening displacement (CMOD) were measured by the means of load cell and two LVDT gauges, respectively (Fig. 6.7). The splitting force (F_h), horizontal component of the force acting on the rollers (Fig. 6.8), is an important parameter since it directly results in a crack opening in the sample and therefore has to be determined to calculate the WST specific fracture energy.

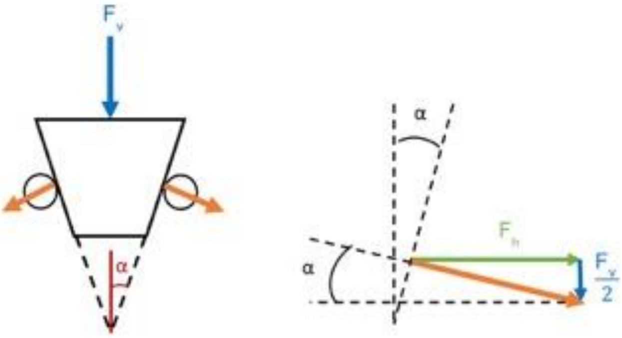

Fig. 6.8 - WST free-body diagram of forces

Considering the wedge angle (α), 7.5° in this research, the F_h is calculated using the equation (1):

$$F_h = \frac{F_v}{(2.\tan\alpha)} \tag{1}$$

The work of fracture (W_f) representing the area under the F_h-CMOD curve, divided by the projected fracture area (ligament area) gives the specific fracture energy (G_f) as described in the equation (2):

$$G_f = \frac{W_f}{A_{lig}} = \frac{1}{(W - a_0)B} \int P_h d\delta_h \qquad (2)$$

Where,

W: sample depth;
a: initial notch length;
B: sample thickness;
F_h : splitting applied load;
δ: is the horizontal displacement of the load point (CMOD)

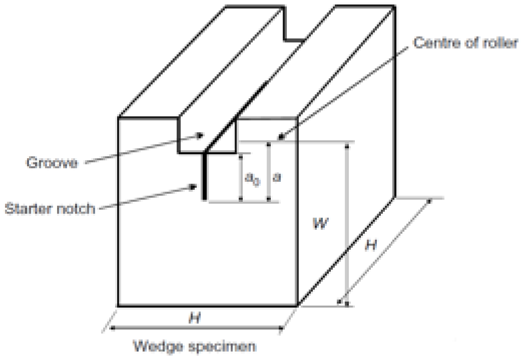

Fig. 6.9 - WST sample (Wen et al. 2012)

The **bi-surface shear test** is a method used to measure the shear bond strength. This method was first developed by (Momayez et al., 2004) in which the cubic composite specimen with the overlay-to-substrate height ratio of 1:2 is subjected to a compressive force. As shown in Fig. 6.10, the compressive loading induces two shear planes, one located along the interface and the other one within the substrate concrete with high shear strength, making the shear failure likely occurring along the interface. Compared to other shear test methods, this test has introduced advantages such as symmetrical loading, easy fabrication without requiring special forms or cutting procedure, as well as simulating a state of stress closer to that of real conditions (Momayez et al., 2004).

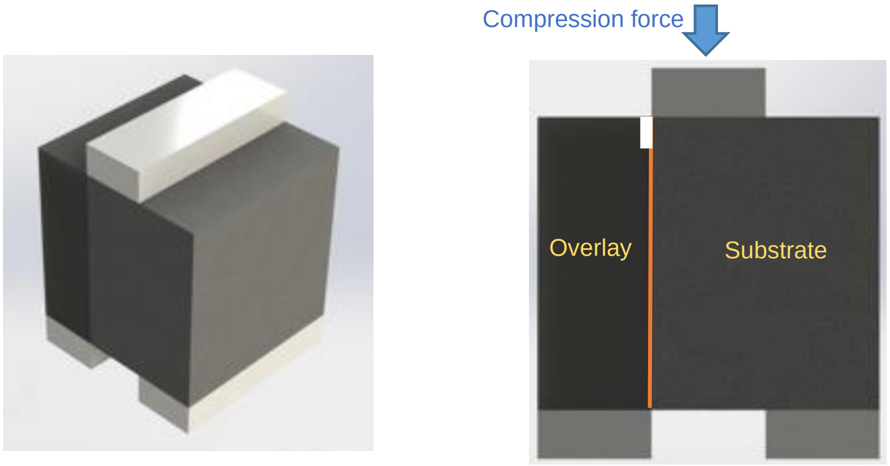

(a) **(b)**

Fig. 6.10 - Bi-surface shear test setup; ***(a)*** *3D model* ***(b)*** *cross section*

In this study, three replicate samples were cut from each composite plate. The samples were 9×5×5 cm^3 prisms, where 6 cm of the sample comprised the concrete substrate, and the 3 cm consisted of the overlay. Based on previous experiences, a notch with a depth of 1.5 cm was sawed along the interface to enforce the crack propagation at the interface. As shown in Fig. 6.11, the sample was placed on top of two linear steel plates, one beneath the overlay in such a way that its edge is below the interface, and the other beneath the substrate layer, symmetrically. The compressive load was exerted through another steel plate placed on the top of the sample. Upon performing the test, the value of failure shear force (maximum force) was measured for each sample. Dividing this value by the shear plane (ligament area) gives the interfacial shear strength.

Fig. 6.11 - Bi-surface shear test experiment

Samples identification

The composite specimens were labeled considering (1) the type of experimental test method; (2) the number of the specimen; (3) the induced temperature; (4) the characteristic compressive strength of the substrate layer. Depending on the test method used, the specimens were denoted by “P” for pull-off test, “W” for wedge splitting, and “S” for bi-surface shear test. The specimens were also tagged with the capitals “L” for low strength (C30/37) concrete substrate layer and “H” for high strength (C45/55) concrete substrate layer. For instance, in the pull-off test, the second replicate of a specimen subjected to the temperature of 35 °C with a concrete substrate layer type of C30/37 was denoted by 35-P-2-L.

Results and discussion

In this section, the experimental results of pull-off tests, wedge splitting tests, and bi-surface shear tests will be presented and discussed.

Pull-off test

Fig. 6.12 indicates the results of pull-off tests for each composite plate. Reproducible results were observed for the replicate samples of each composite plate and the standard deviation values were less than 0.25 MPa for all specimens.

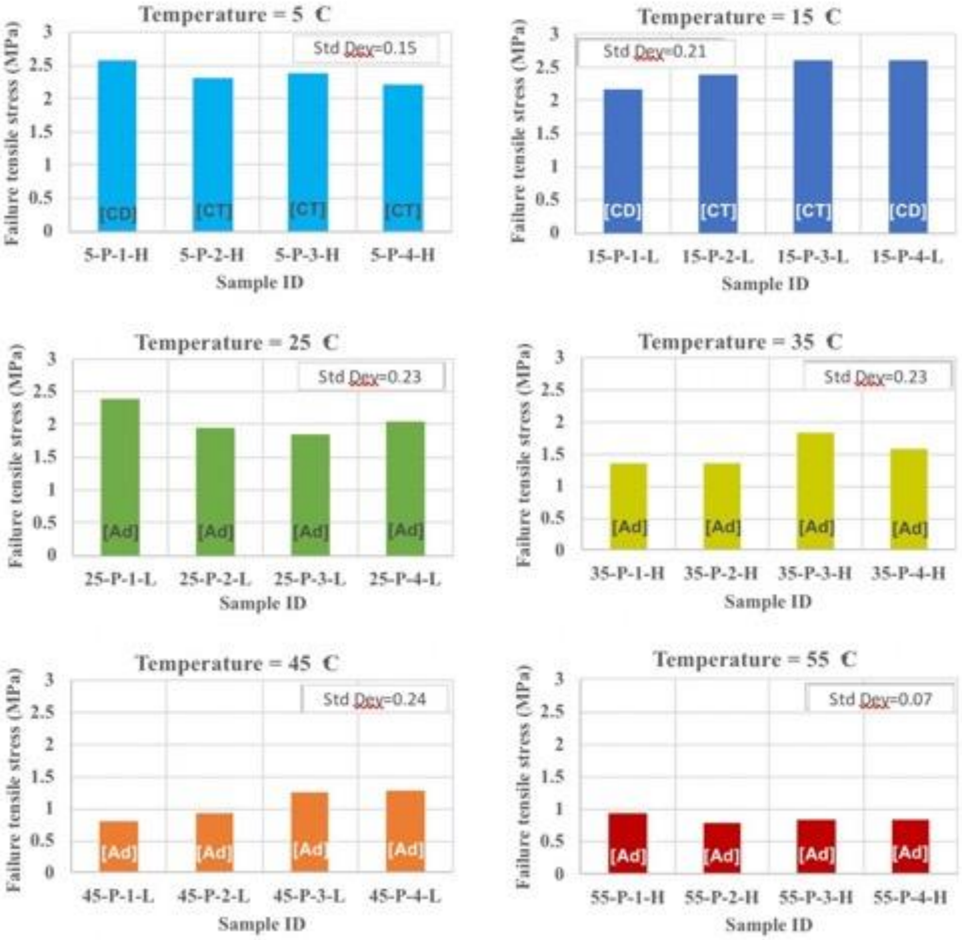

Fig. 6.12 - Failure tensile stress measured with pull-off test for all samples. The first number indicates the temperature of conditioning and early curing of the sample.

Depending on the location of failure in the pull-off test, four different types of failure can occur as shown in Fig. 6.13.

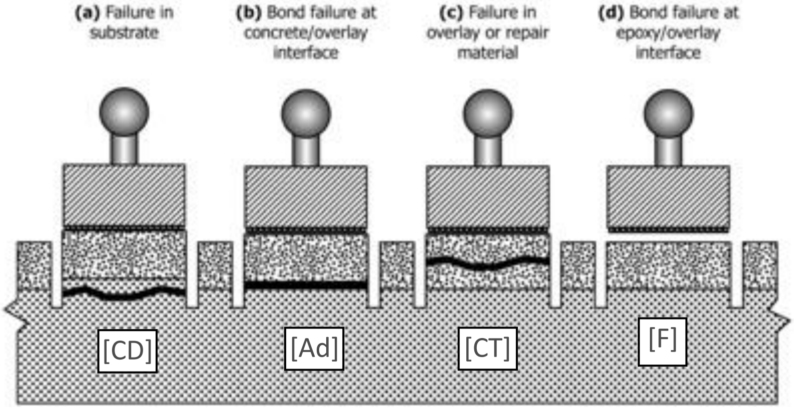

Fig. 6.13 - Different failure modes in the pull-off test (ASTM C1583 / C1583M-20, 2020). Our classification refers to [CD] for substrate (down) concrete cohesive failure, [Ad] for concrete-concrete interface failure, [CT] for the overlay (top) concrete cohesive failure and [F] means failed test, as the failure occurred in the setup.

According to this classification (we only changed the name), the observed failure mode in each sample was also tagged in Fig. 6.12. It should be noted that for the samples indicating the failure at the bond line between the steel disk and the epoxy adhesive, the test was repeated as recommended by the standards (ASTM C1583 / C1583M-20, 2020). Our results show that the adhesive failure [Ad] along the interface occurred mostly in the samples subjected to the higher temperature values, while at lower temperature values (5 and 15 ºC), cohesive failure [CD] or [CT] within the substrate or overlay happened. The failure modes reveal that the interfacial bond strength will become weaker compared to the bulk concrete if the conditioning temperature is increased. It is noteworthy to mention that due to the high interfacial bond strength and hence failure in the bulk concrete, the reported failure tensile stress values in 5 and 15 ºC only gives a lower estimation of the interfacial bond strength.

Looking at samples 5-P-H and 15-P-L, for which all failures were cohesive, either in substrate or in overlay, we can conclude that the concrete type used in the substrate layer does not seem to play a large role on the failure location.

To quantify the effect of temperature on the tensile bond strength, the mean failure tensile stress was computed for each composite specimen and plotted in Fig. 6.14. Results clearly show that the conditioning and early curing temperature highly affects the bond strength. Pull-off results show that increasing the temperature from 5 to 55 ºC results in lowering the tensile bond strength from 2.35 ± 0.15 to 0.85 ± 0.07 MPa, a 64% reduction in tensile strength. This decreasing trend is consistent with the type of failures observed in each specimen as described before: At low temperature, the failure is cohesive (it happens in the bulk) and upon increasing temperature, the failure occurs at the interface for all samples. The low standard deviation values confirm the reliability of the data.

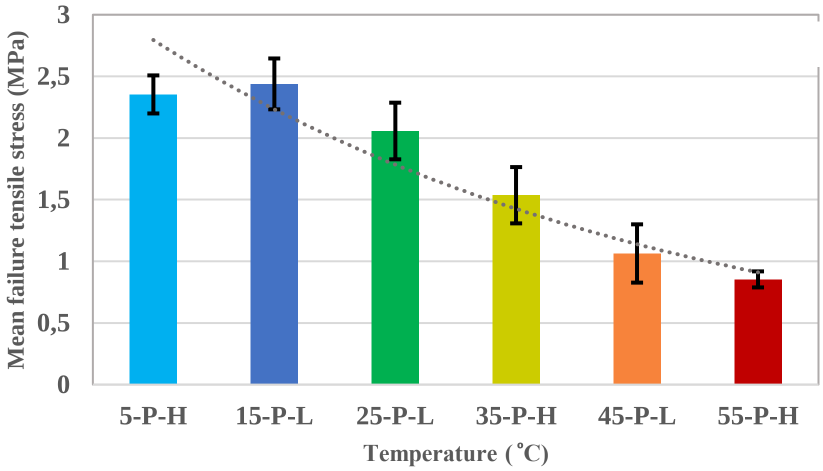

Fig. 6.14 - Mean failure tensile stress measured with pull-off test function of conditioning/early curing temperature (indicated by the first number on the specimen series name). The dotted line represents the exponential regression line.

Wedge splitting test (WST)

A typical F_h-CMOD curve obtained in this study is plotted in Fig. 6.15. Unlike brittle materials with a sharp drop in the load-displacement, the F_h-CMOD curves in this study were smooth for almost all the samples, indicating a stable crack propagation (i.e. of the load stops, the crack stops propagating) and slow unloading process in the post-peak area. The early part of the curve represents the sample loading (no crack propagation). Upon reaching the peak load value, i.e. post-peak load area, the crack becomes critical and starts to propagate. It is noteworthy to mention that the strain-softening behavior was observed in the F_h-CMOD curves of all the samples revealing the quasi-brittle behavior of the tested concrete in this research.

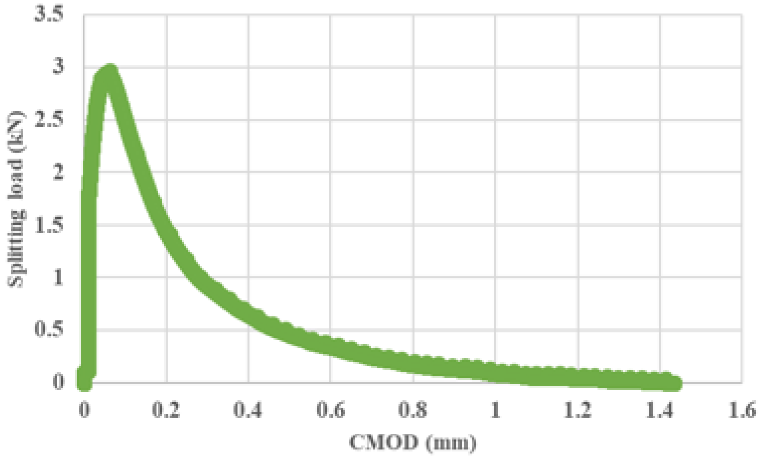

Fig. 6.15 - Typical load-displacement curve in the WST (Sample: 25-W-2-L)

The types of failure in the WST reveal useful information regarding the interfacial bond strength. In this regard, 4 different types of failure observed in the WST were classified based on their location and denoted as follows: the concrete-concrete interface [Ad], the overlay concrete [CT], the substrate concrete [CD] and both the interface and substrate concrete [CDA]. These failure modes tag each sample in Fig. 6.16.

The values of peak splitting loads were calculated and plotted in Fig. 6.16. The standard deviation values were calculated and are less than 0.6 kN for all the specimens. However, compared to the pull-off test results, a larger data dispersion was observed in the WST results. As reported by (Brühwiler & Wittmann, 1990), the WST is size-dependent, and therefore small differences (< 0.1 cm) between the dimension of the replicate samples, especially the notch depth, will result in dispersion in the data. It should be noted that testing the fourth replicate sample of the composite conditioned at the 25 ºC, namely 25-W-4-L, was unsuccessful for three times and hence was omitted from the results.

The mean WST peak splitting load for each composite specimen is plotted in Fig. 6.17. Similarly, as in the pull-off tests, the effect of temperature is important and the samples conditioned at lower temperature values (5, 15, and 25 ºC) show higher peak splitting load and therefore present higher fracture resistance. Results reveal that increasing the temperature from 5 to 55 ºC results in lowering the WST peak splitting load from 2.7 to 1.5 kN, i.e. 44% reduction in the peak splitting load. In contrary to the pull-off test results, the type of substrate concrete affects the failure mode, i.e. more cohesive failure within the overlay was observed when a stronger substrate was employed and vice versa. This can also explain the lower mean peak splitting load observed in the 5-W-H samples (failure in weaker overlay) compared to that of 15-W-L. For both samples, the peak splitting load gives a lower bond estimation of the bond strength.

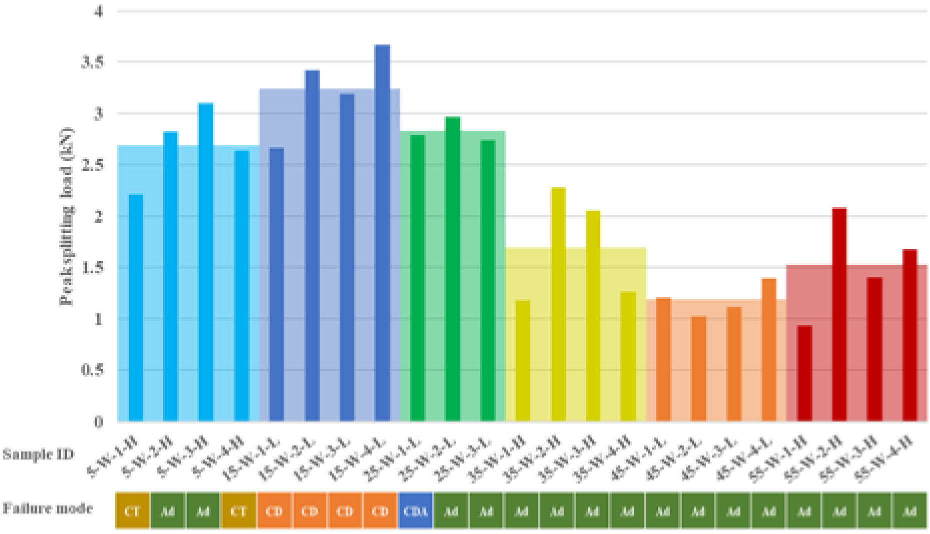

Fig. 6.16 - Peak splitting load measured with wedge splitting test for all samples; CT indicates cohesive failure in the overlay, CD indicates cohesive failure in the substrate, Ad indicates adhesive failure along the interface and CDA indicates a simultaneous adhesive and cohesive failure in the substrate

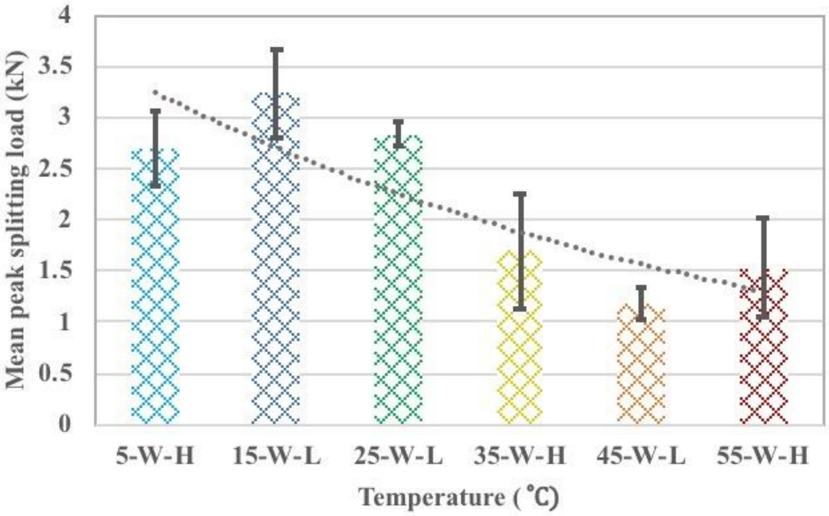

Fig. 6.17 - Mean peak splitting load measured with WST test function of conditioning/early curing temperature (indicated by the first number on the specimen series name). The dotted line represents the exponential regression line.

On top of measuring peak load values, which determines the cracking resistance of the samples, the specific fracture energy was also calculated.

As described before, the CMOD values were collected by the means of two different LVDT gauges measuring the displacement from two sides of the samples (Fig. 6.7). With these two distinct measurements, it is possible to find out how the crack propagates in the two sides of the sample and check if the test is symmetric, as expected. To take this into consideration, three specific fracture energy values were calculated for each sample based on two distinct CMODs and also their average value. The specific fracture energy was computed based on eq. (2), and plotted in Fig. 6.18. As shown, there were no remarkable difference between the three specific fracture energies calculated for each sample and hence, this reveals the reproducibility and validity of the CMOD measurements in this study. Moreover, although reproducible results were obtained for samples of each composite plate, there was more data dispersion compared to the pull-off test and WST peak splitting load. Both the WST size dependency and the error in displacement measurements due to non-perfect alignment of the samples are the main reasons for larger data dispersion.

Here again, at low temperatures, especially 5 and 15 ºC, more cohesive failures within the bulk concrete were observed. This reveals that in the lower temperature value the interfacial bond strength was stronger compared than that of bulk concrete and hence the crack deviates and propagates in the concrete.

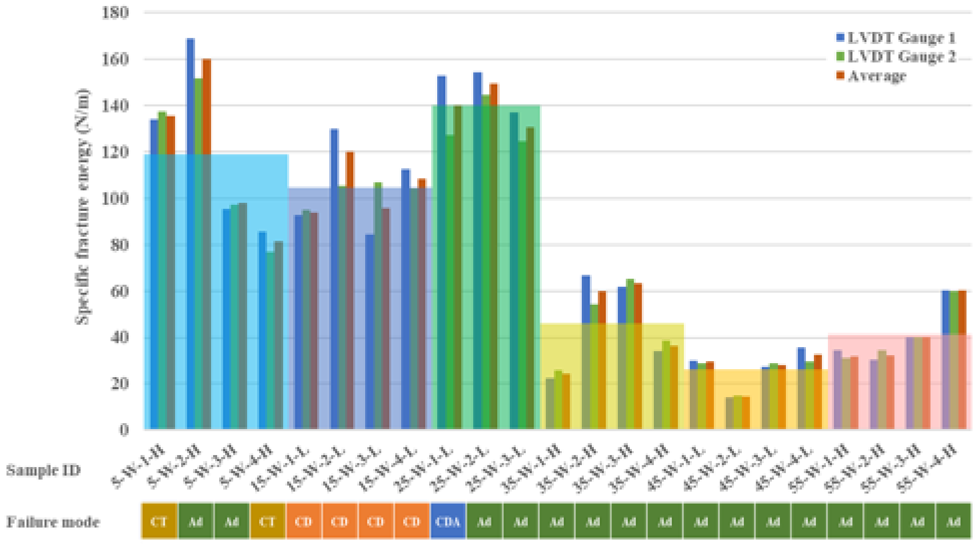

Fig. 6.18 - Specific fracture energy measured with wedge splitting test for all samples; CT indicates cohesive failure in the overlay, CD indicates cohesive failure in the substrate, Ad indicates adhesive failure along the interface and CDA indicates a simultaneous adhesive and cohesive failure in the substrate

The mean WST specific fracture energy was computed for each composite specimen and plotted in Fig. 6.19. Here again, the conditioning and early curing temperature affects the bond strength. WST results show that increasing the temperature from 5 to 55 ºC results in lowering the WST specific fracture energy from 119 ± 36 to 41 ± 13 (N/m), a 65% reduction in the specific fracture energy. Like in previous results, the calculated specific fracture energy of samples with cohesive failure only gives a lower estimation of the real interfacial bond strength. This explains the lower WST specific fracture energies in the 5-W-H and 15-W-L specimens compared to that of 25-W-L with at least 67% adhesive failures. This decreasing trend is consistent with those observed for WST failure modes and results of pull-off tests.

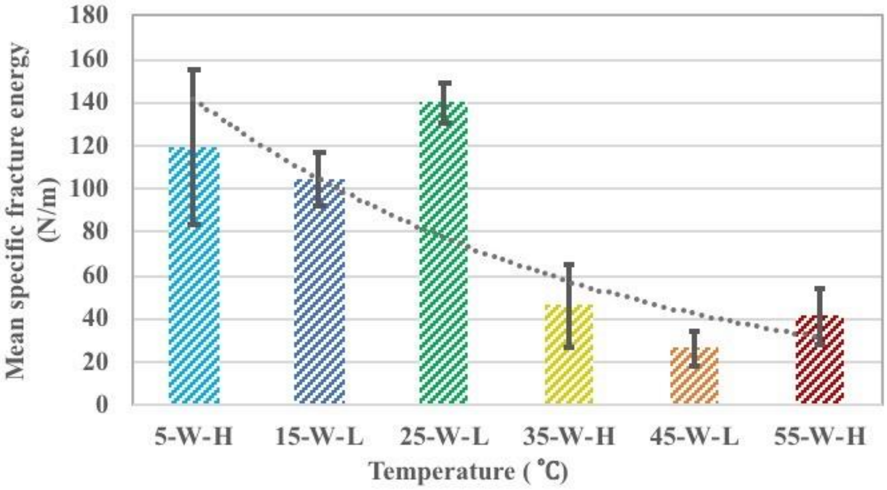

Fig. 6.19 - Mean specific fracture energy measured with WST test function of conditioning/early curing temperature (indicated by the first number on the specimen series name). The dotted line represents the exponential regression line.

Bi-surface shear test

Fig. 6.20 presents the results of the effect of temperature on the shear bond strength. In these tests, all observed shear failures occurred along the interface, due to the presence of the notch. Results show that here again, the conditioning and early curing temperature affects the bond strength. When increasing temperature from 5 to 55 ºC, the shear bond strength reduces from 11.6 ± 0.7 to 7.3 ± 2.1 MPa, i.e. a 37% reduction. Although this decreasing trend is consistent with the results of pull-off and wedge splitting tests, the reduction value was less than that of pull-off and WST demonstrating the lower impact of temperature on shear bond strength. The authors attribute this to the fact that friction and interlocking are the main load-carrying mechanisms under shear and these are not susceptible to the temperature.

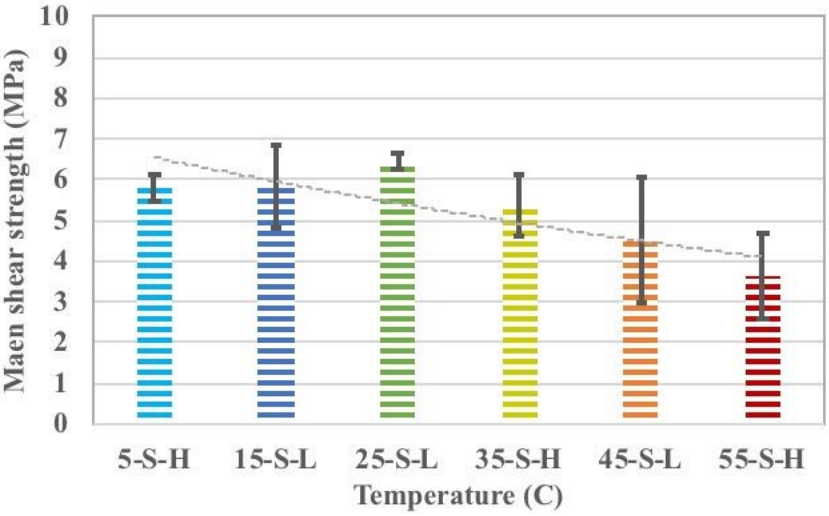

Fig. 6.20 - Mean shear strength measured with bi-surface shear test function of conditioning/early curing temperature (indicated by the first number on the specimen series name). The dotted line

represents the exponential regression line.

Conclusion

In this work, the effect of temperature, as one of the most important environmental factors on the interfacial bond strength, has been investigated. Samples were prepared at six different temperature values, covering a range from 5 to 55 ºC. The interfacial bond strength of the conditioned composites was then tested under various states of stress at room temperature, simulating the real conditions. Based on the experimental results, the following conclusions were drawn:

- The conditioning and early curing temperature highly impacts the bond strength. Increasing the temperature from 5 to 55 ºC results in lowering the interfacial bond strength by 64% in tension, by 37% in shear, and by 65% in fracture crack opening mode.
- The lower reduction in the shear strength compared to that of pull-off and wedge splitting tests demonstrates the load-carrying mechanism in the interfacial shear strength is less influenced by the bonding agent (and therefore by the temperature) than the tests where the interface is subjected to tension.
- A greater number of failures occurred within the bulk concrete (cohesive failure) for samples prepared at lower temperatures. This confirms that lower temperature values cause higher interfacial bond strength.
- The type of concrete making the sublayer (compressive and tensile strength) only lightly affected the failure modes in the pull-off and bi-surface shear test, as both substrate and overlay failure were observed in the tests. On the other hand, the type of substrate concrete affects the WST failure modes, i.e. more cohesive failure within the overlay was observed when a stronger substrate was employed and vice versa

Perspectives

Although this experimental campaign revealed the negative effect of high-temperature values on the interfacial bond strength, it is still unclear how the temperature affects the interfacial load-carrying mechanism. Therefore, further investigation is planned on the mechanical properties of epoxy under different conditioning/early curing temperatures to find out how they are affected. The micrography of the interface is also planned that will provide a clear insight about the epoxy distribution near the interface under different temperature values.

Next, the project will focus on sloped floors/pavements, planning on quantifying the effects of differential shrinkage and thickness variation. this project aims at providing a practical guideline in terms of sloped floors/pavements performance proposing proper technical actions to prevent the shrinkage cracking and improve their mechanical properties.

References

ASTM C1583 / C1583M-20. (2020). ASTM International, West Conshohocken, PA, 2020

Brühwiler, E., & Wittmann, F. H. (1990). *Engineering Fracture Mechanics*, *35*(1–3), 117–125. https://doi.org/10.1016/0013-7944(90)90189-N

Emmons, P. H. (1994). *Concrete Repair and Maintenance Illustrated*. R. S. Means Company.

He, Y., Zhang, X., Hooton, R. D., & Zhang, X. (2017). *Construction and Building Materials*, *151*, 582–590. https://doi.org/10.1016/j.conbuildmat.2017.05.049

Júlio, E. N. B. S., Branco, F. A. B., Silva, V. D., & Lourenço, J. F. (2006). *Building and Environment*, *41*(12), 1934–1939. https://doi.org/10.1016/j.buildenv.2005.06.023
Li, G. (2003). *Cement and Concrete Research*, *33*(6), 799–806. https://doi.org/10.1016/S0008-8846(02)01064-5
Linsbauer, H. N., & Tschegg, E. K. (1986). *Zement Und Beton*, *31*(1), 38–40.
Momayez, A., Ehsani, M. R., Ramezanianpour, A. A., & Rajaie, H. (2005). *Cement and Concrete Research*, *35*(4), 748–757. https://doi.org/10.1016/j.cemconres.2004.05.027
Santos, D. S., Santos, P. M. D., & Dias-Da-Costa, D. (2012). *Construction and Building Materials*, *37*, 102–110. https://doi.org/10.1016/j.conbuildmat.2012.07.028
Santos, P. M. D. (2010). 2010 *3rd Fib International Congress*, *November*.
Santos, P. M. D., & Júlio, E. N. B. S. (2013). *Construction and Building Materials*, *38*, 912–923. https://doi.org/10.1016/j.conbuildmat.2012.09.045
Silfwerbrand, J. (1990). *Concrete International*, *12*(9), 61–66.
Zanotti, C., & Randl, N. (2019). *Cement and Concrete Composites*, *99*(February), 80–88. https://doi.org/10.1016/j.cemconcomp.2019.02.012
Zhang, Y., Zhu, P., Liao, Z., & Wang, L. (2020). *Construction and Building Materials*, *235*, 117431. https://doi.org/10.1016/j.conbuildmat.2019.117431

WORK PACKAGE 7

Device for measuring infiltration

The thermal insulation of a material is linked to its content in air, i.e. its porosity. For example, expanded polystyrene designed for thermal insulation purpose has densities between 11 - 30 kg/m^3, corresponding to thermal conductivity of 0.029 - 0.044 W/mK. This corresponds to polystyrene content of 1-3%. In other words, these foams contain 97-99% of air.
Cement foams may reach densities as low as 50 kg/m^3. This corresponds to a solid content of approximately 2 %. Such foams have very low mechanical properties.
In this project, we explore the manufacturing of light and insulating material by infiltrating a bead of porous clay beads with a cement slurry. We investigate both types of LECA beads (large 8-16mm) and small (4-8 mm).

The first version of the setup consisted in a beaker full of LECA beads.
A cement slurry was prepared with CEM I, a water-to-cement ratio of 0.4, and superplasticizer ACE 430 0.35 % bwoc.
Such a slurry infiltrated a 30 cm high pack of large and prewetted (fully saturated in water) LECA beads (Fig. 7.1) but could not infiltrate the same pack made with the small LECA beads (Fig. 7.2).

Fig. 7.1 – Pre-wetted large LECA beads infiltrated by a cement slurry placed from top. Infiltration was successful as all beads are surrounded by cement.

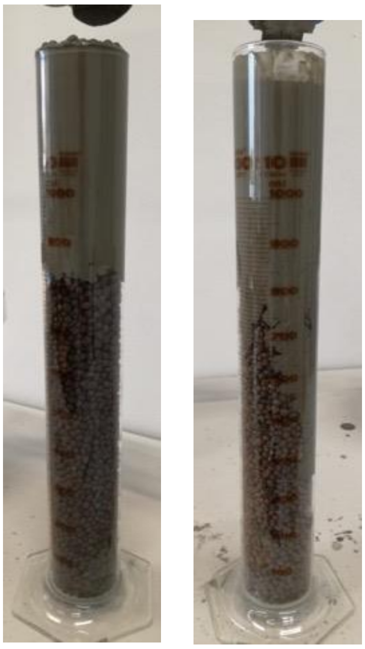

Fig. 7.2 – Pre-wetted small LECA beads partially infiltrated by a cement slurry placed from top.

Infiltration was not successful as not all beads are surrounded by cement.

The setup with infiltration from bottom is being designed. It involves 2 series of large transparent pipes of internal diameters of 144 mm and 94 mm. The ratios between the pipe internal diameter (ID) and the beads size is shown in Tab 7.1. This ratio stays on average above 10. This helps mitigate the effect of the wall by geometrical steric effects.

Tab. 7.1 - Ratios between the pipe internal diameter (ID) and the beads size

LECA Beads	Pipe iD (144 mm) / bead size	Pipe ID (94 mm) / bead size
4-8 mm	18 - 36	12 - 24
8-16 mm	9 - 18	6 - 12

Pressure sensors were ordered, see Fig. 7.3.

Fig. 7.3 – Pressure sensors purchased for the construction of the infiltration setup.

The setup is shown Fig. 7.4. Cement slurry will be pumped from bottom and the fluid propagating front will be measured with time.

Parameters of the experiment include: particle diameter, pipe diameter, cement slurry rheological properties.

Fig. 7.4 – Picture of infiltration setup from bottom.

WORK PACKAGE 8

Equipment for the production of cement foams

Results and literature review from year 1 have shown that foam stability is a critical aspect of producing cement foams, as most surfactants are negatively influenced by the presence of calcium ions and that C-S-H particles may stabilize the foam while having a positive effect on its set mechanical properties. Also, a high yield stress slurry may have positive influence on foam stability, and fast setting will diminish the impact of stability issues. For all these reasons, we decided to procure and start testing a C-S-H paste. It means the capacities of this work package were mostly moved to WP 5. The foaming setup, on the other hand, is considered less critical, and the focus of a setup that involves similar controls (flow and pressure) is being built in work package 7. Therefore, the capacities of this work package were also partially moved to WP 7.

Preliminary results of characterization of a C-S-H are below. Oscillatory rheology was performed with the goal of quantifying inter-particle forces.
The C-S-H paste is shown Fig. 8.1, after having been tested on the rheometer.
Early and preliminary rheology results show that the C-S-H paste exhibits lower small strain elastic modulus (stiffness) than fresh cement.

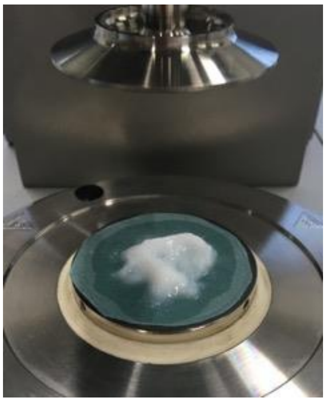

Fig. 8.1 – Paste of C-S-H, the main hydration product of cement, after a rheological test.

WORK PACKAGE 9

Device for characterizing volume changes or limiting pressure of RA concretes

It was decided to focus on the effect of gypsum as a problematic residual ingredient present in recycled aggregates. Internal sulfate attacks have indeed been far less studied than external sulfate attacks. Our goal is to bring more data that could support consolidated guidelines for the use of recycles aggregates at the European level.

A set of experiment was started, that focused on the effect of the presence of gypsum in concrete. Parameters include water-to-cement ratio, gypsum content, size of gypsum particles, and temperature. Expansions were followed measuring the length of a 25 x 25 x 285 mm^3 sample (ASTM C452-06 / C1038-04), and using Le Chatelier rings (ASTM C452). Swelling pressures were measured using an oedometer.

Length measurements were done using the device shown Fig. 9.1. Samples were measured immediately after demolding, and then at time intervals after concrete hydration and during aging in water at various temperatures.

Fig. 9.1 – Setup for concrete sample length measurement

For these tests, CEM I 52.5 R (Der Blaue) was selected. Ordinary modeling plaster was mixed with water, left to hydrate and then crushed and sieved to get two different grades: fine grained plaster (<1mm) and coarse grained plaster (1-4mm) (Fig. 9.2).
Mixtures where prepared with water-to-cement ratios of 0.5 and 0.65, added gypsum content of 0, 5 and 10%, and sand of approximately 60 w%. See compositions in Tab. 9.1.

Fig. 9.2 – Pictures of obtained fine-grained plaster (left) and coarse-grained plaster (right)

Tab. 9.1 - Overview of the ten mixtures for the main test series

Name of the sample	Water quantity in [g]	Amount of cement in [g]	Sand quantity in [g]	Plaster quantity in [g]
0k0,5	225	450	1350	0
0k0,65	292,5	450	1350	0
5f0,5 / 5g0,5	225	450	1327,5	22,5
5f0,65 / 5g0,65	292,5	450	1327,5	22,5
10f0,5 / 10g0,5	225	450	1305	45

10f0,65 / 10g0,65	292,5	450	1305	45

Le Chatelier-Astett-Test uses hydrated cement particles, mixed with plaster and water. Three different cement were tested to compare their reactivity to gypsum. All were mixed, hydrated and then grinded. Particle size distribution was measured using the Mastersizer 3000 device. Results are shown in Table 9.2.

Tab. 9.2 – Particle size distribution measured on all grinded specimen used in Chatelier-Astett-Test

Name of the sample	Dx (10) in [µm]	Dx (50) in [µm]	Dx (90) in [µm]
"The Blue" CEM I 52,5 R	6,42	16,3	174
"The Contragress" CEM I 52.5 N - C3A-free	5,83	15,4	82,3
Supracem 45 fast-hardening cement	3,22	16,5	111
Plaster	7,87	166	415

The particles of hydrated cement were then mixed with plaster particles and water, and the slurry filled in Le-Chatelier needle rings, Fig. 9.3.

Fig. 9.3 – Picture of the Le Chatelier ring

Finally, similar mixtures were tested in an oedometer. In this case, the sample is submitted to full confinement, and the pressure it exerts against its confinement is measured. A WILLE oedometer was used, see Fig. 9.4.

Fig. 9.4 – Picture of the WILLE oedometer used for this series of experiments

Samples were similar to samples prepared for the Le Chatelier-Astett tests, but only the dry powders were mixed and compressed. The samples after being placed in the mold and slightly compressed, are exposed to water, and pressure resulting from physical and chemical reactions is recorded.

3. Project team and cooperation

- Are there significant changes in the project team (internal key staff and external partners/third parties)?
- Address changes in the division of labour.
  Are there any effects on the cost / financing structure and the target?

Subhransu Dhar, Projektassistent, wurde mit 2. März 2020 angestellt.
Roland Stöttner hat das Projektteam verlassen.

4. Economic and scientific exploitation

- Describe the exploitation and / or redistribution activities carried out so far.
  Is exploitation possible?
- List publications, dissertations, theses and any patent applications, which have arisen from the project.
- What further R&D activities are planned?
- How will the prototypes created in the project be further used?

Are alkali activated binders intermediate between cement and mineral suspensions?, T. Liberto, M. Bellotto, A. Robisson, 29th international Conference on Rheology of Building Materials, OTH- Regensburg, Germany March 11 - 12, 2020

5. Explanations on costs & financing

- Billing is done directly in eCall or, for projects submitted by Sept. 2015, via Excel. In eCall you will automatically be presented with the right variant for you.
- Please refer to the FFG cost guidelines (www.ffg.at/kostenleitfaden) and tender documents.
- Deviations from the cost plan must be described and justified at this point.

6. Project specific special conditions and requirements

- Deal with project-specific special conditions and requirements (according to §6 of the Grant Agreement), if these have been agreed in the Grant Agreement or Contract for Work and Labor.

7. Notifiable events

Are there any special events relating to the funded project which must be notified to the FFG (see also Guidelines - Annex to 5.3., 5.3.5), e.g.

- Changes in the legal and economic possibilities of influencing the Recipient
- Insolvency proceedings
- events that delay the performance of the subsidised service, or
  render impossible
- Further funding for this project